Acta Geologica Polonica, Vol. 68 (2018), No. 1, pp. 53–88
DOI: 10.1515/agp-2017-0031

From museum drawers to ocean drilling: *Fenneria* gen. nov. (Bacillariophyta) offers new insights into Eocene marine diatom biostratigraphy and palaeobiogeography

JAKUB WITKOWSKI

Stratigraphy and Earth History Lab, Faculty of Geosciences, University of Szczecin, Mickiewicza 16a, PL-70-383 Szczecin, Poland. E-mail: jakub.witkowski@usz.edu.pl

ABSTRACT:

Witkowski, J. 2018. From museum drawers to ocean drilling: *Fenneria* gen. nov. (Bacillariophyta) offers new insights into Eocene marine diatom biostratigraphy and palaeobiogeography. *Acta Geologica Polonica*, **68** (1), 53−88. Warszawa.

Triceratium barbadense Greville, 1861a, *T. brachiatum* Brightwell, 1856, *T. inconspicuum* Greville, 1861b and *T. kanayae* Fenner, 1984a, are among the most common diatoms reported worldwide from lower to middle Eocene biosiliceous sediments. Due to complicated nomenclatural histories, however, they are often confused. A morphometric analysis performed herein indicates that *T. brachiatum* is conspecific with *T. inconspicuum*, and that both were previously often misidentified as *T. barbadense*. *Triceratium barbadense sensu stricto* is a distinct species similar to *Triceratium castellatum* West, 1860. *Triceratium brachiatum* and *T. kanayae* are transferred herein to a new genus, *Fenneria*, for which a close phylogenetic relationship with *Medlinia* Sims, 1998 is proposed. A review of the geographic and stratigraphic distribution of *Fenneria* shows that the best constrained records of its occurrences are found at DSDP Site 338, and ODP Sites 1051 and 1260. The ages of the base (B) and top (T) of each species' stratigraphic range are calibrated here to the Geomagnetic Polarity Timescale either directly or inferred via correlation with dinocyst biostratigraphy. Latitudinal diachroneity of ~7 million years is documented for *F. brachiata*, which disappears earlier in tropical and mid-latitude sites than in the northern high latitudes. These observations, coupled with a preliminary compilation of the Chron C20n taxonomic composition of pelagic diatom assemblages for Sites 338, 1051 and 1260, indicate that diatoms diversified palaeobiogeographically considerably earlier than the Eocene−Oligocene Transition, as commonly believed. This study also emphasizes the importance of the detailed examination of specimens from both museum collections and deep-sea cores as a step toward enhancing the utility of Palaeogene diatoms in palaeoceanographic and palaeoenvironmental reconstructions.

Key words: *Triceratium barbadense*, *Triceratium brachiatum*, *Triceratium inconspicuum*, *Triceratium kanayae*, Palaeogene, fossil diatoms, taxonomy, biostratigraphy, palaeobiogeography

INTRODUCTION

Palaeogene diatoms

Numerous lines of evidence suggest that the Palaeogene Period (~66−23 Ma; Gradstein *et al.* 2012) witnessed the rise of marine diatoms to ecological prominence (Egan *et al.* 2013; Lazarus *et al.* 2014; Barron *et al.* 2015; Renaudie 2016). *Triceratium* Ehrenberg, 1839 is often cited as one of the most common Palaeogene diatoms (e.g., Strelnikova 1992). For most of the 19th and 20th centuries, *Triceratium*

was subject to divergent taxonomic interpretations, and numerous workers made attempts to establish its generic limits (e.g., Ross and Sims 1971; Gleser 1975, 1986; Sims and Ross 1990; Sims and Hendey 2002). Both morphological and molecular data (Ashworth *et al.* 2013; Witkowski *et al.* 2015), however, suggest that *Triceratium sensu lato* remains a heterogeneous collection of taxa. This taxonomic confusion greatly hinders the geological utility of the entire group, which likely comprises several hundred species.

Most reports on early to middle Eocene diatoms mention one or more of three globally distributed species: *Triceratium brachiatum* Brightwell, 1856, *Triceratium barbadense* Greville, 1861a, and *Triceratium inconspicuum* Greville, 1861b (Text-figs 1, 2). Wherever illustrations are provided, these species appear to closely resemble each other; yet, numerous workers made attempts to distinguish between these taxa morphologically (e.g., Fenner 1977, 1985; Baldauf and Pokras 1989; Renaudie *et al*. 2010), and even ecologically (e.g., Radionova 1996).

Triceratium barbadense, *T. brachiatum* and *T. inconspicuum* are often reported together with *Triceratium kanayae* Fenner, 1984a (e.g., Barron *et al*. 1984; Fenner 1985; Renaudie *et al*. 2010; Witkowski *et al.* 2012a). Although valves of all these taxa commonly measure less than 20 μm, light microscope examination reveals that they have poroid valves with no ocelli or pseudocelli, prominent internal costae that are not involved in girdle attachment, minute rimoportulae, and prominent serrations on the mantle margin. As demonstrated here, these morphological features warrant the erection of a new genus, *Fenneria* gen. nov.

Despite their high diversity and wide distribution in both deep-sea and onshore sites, Palaeogene diatoms are greatly understudied in comparison to foraminifers, calcareous nannofossils, dinocysts and radiolarians. Despite the wealth of literature on low-latitude and southern high latitude Palaeogene diatom biostratigraphy (e.g., Gombos 1982a; Fenner 1984a; Fourtanier 1991; Harwood and Maruyama 1992; Scherer *et al*. 2007; Barron *et al*. 2014, 2015), modern biostratigraphic concepts such as the diachroneity of diatom zonal boundaries have not been considered to date. *Triceratium barbadense*, *T. brachiatum*, *T. inconspicuum* and *T. kanayae* are all regarded as useful stratigraphic markers for lower to middle Eocene low-latitude sediments (Fenner 1984a; Scherer *et al.* 2007; Barron *et al*. 2015). However, the taxonomic confusion and incomplete understanding of their stratigraphic and geographic distribution limits their full potential in biostratigraphic and palaeoceanographic studies.

Aims of this study

This paper aims at: 1) establishing whether or not *T. barbadense*, *T. brachiatum*, and *T. inconspicuum* are conspecific; 2) proposing *Fenneria* gen. nov., and providing a detailed account of its morphology; and 3) compiling new and published data from a range of deep-sea and onshore sites in order to improve the biostratigraphic utility of *Fenneria* gen. nov.

Additionally, this study attempts an overview of the current status of the Palaeogene diatom field, and the direction of its future development. As advocated here, integration of data from shallow-water and pelagic sites, combined with careful morphological examination of specimens, including those from type materials, has the potential to enhance Palaeogene diatom utility in biostratigraphy and palaeoceanography. This is especially important given the recent renewed interest in fossil diatoms as palaeoproductivity proxies (e.g., Davies *et al*. 2009, 2012; Witkowski *et al.* 2012a, 2014; Renaudie 2016) that could provide new insight into the links between primary production and organic carbon burial as drivers of both long- and short-term Palaeogene climatic shifts.

MATERIALS AND METHODS

Sources of specimens

This study is based on specimens examined by means of scanning electron microscope (SEM), and/or light microscope (LM), and a compilation of published records based on literature survey. A brief list of sites examined and referenced herein (Text-fig. 1) is given in Table 1. Specific details on the location, stratigraphy, and previous published reports are presented in the Appendix, along with a complete list of slides examined in this study in the supplementary Tables A1 and A2 in the Appendix.

International deep-sea drilling consortia are abbreviated below as: DSDP (Deep Sea Drilling Project); ODP (Ocean Drilling Program); IODP (Integrated Ocean Drilling Program and International Ocean Discovery Program).

Herbarium codes used below and in the Appendix follow the Index Herbariorum: BM (the Natural History Museum, London, UK) and SZCZ (University of Szczecin, Poland). Additional resources came from the California Academy of Sciences (CAS), and the IODP Micropaleontology Reference Center at University of Nebraska-Lincoln, USA (here abbreviated as MRC).

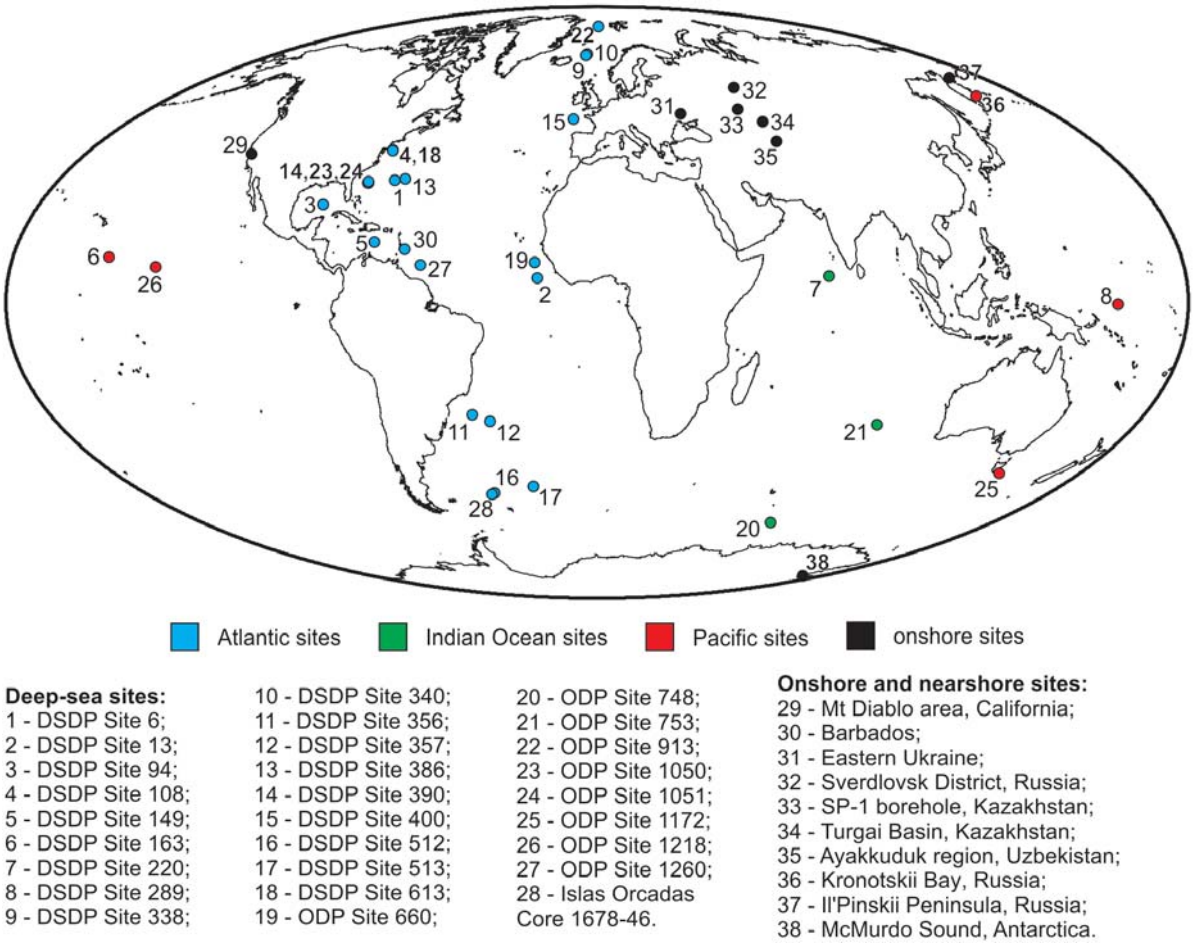

Text-fig. 1. Map showing the localities of diatom records considered in this study. Site numbers correspond to numbers given in Text-figs 5 and 8, and Table 3 (column '#'). For details concerning the stratigraphy of each deposit see the Appendix. For reference see Tables 1 and 3. Base map plotted using the online Ocean Drilling Stratigraphic Network advanced plate tectonic reconstruction application (www.odsn.de)

Age models and biostratigraphy

In order to place the diatom bioevents reported here in a global stratigraphic context and evaluate any potential diachroneity, three sites that combine good diatom preservation with reliable age control were selected along a latitudinal transect: DSDP Site 338 (latitude 67.79º N, 5.39º E), and ODP Sites 1051 (30.05º N, 76.36º W) and 1260 (9.25º N, 54.54º W). Age models were compiled from published magneto- and cyclostratigraphic data for Sites 1051 and 1260, and bio- and magnetostratigraphic data for Site 338 (Table 2). Linear sediment accumulation rates were assumed. Depths for the base (B) and top (T) of stratigraphic ranges of the taxa considered here were established as mid-points between the minimum and maximum depths for the respective events. Ages were calculated for each of these levels by linear interpolation between tie points listed in Table 2. All ages considered in this paper are relative to the Gradstein *et al*. (2012) timescale.

Reproductions

This paper includes reproductions of the original line drawings of *T. barbadense*, *T. brachiatum* and *T. inconspicuum* (Text-fig. 2). High quality scans of the original plates from Brightwell (1856) and Greville (1861a, b) were made using the hardcopies of the *Quarterly Journal of Microscopical Science* and the *Transactions of the Microscopical Society of London* from the BM Libraries. Early issues of both journals are out of copyright. The sizing of scanned images was carefully checked against hardcopies in order to ensure the proper scale of the reproductions.

#	Site	Locality	SEM and LM	LM only	Literature survey
	Deep-sea sites:				
1	DSDP Site 6	Bermuda Rise	+	–	–
2	DSDP Site 13	Sierra Leone Rise	–	–	+
3	DSDP Site 94	Campeche Scarp	–	–	+
4	DSDP Site 108	New Jersey continental slope	–	–	+
5	DSDP Site 149	Venezuelan Basin	–	–	+
6	DSDP Site 163	Clarion Fracture Zone	–	–	+
7	DSDP Site 220	Arabian Basin	–	–	+
8	DSDP Site 289	Northern Ontong Java Plateau	–	–	+
9	DSDP Site 338	Vøring Plateau	–	+	–
10	DSDP Site 340	Vøring Plateau	–	–	+
11	DSDP Site 356	São Paulo Plateau	–	+	–
12	DSDP Site 357	Rio Grande Rise	–	–	+
13	DSDP Site 386	Bermuda Rise	–	+	–
14	DSDP Site 390	Blake Nose	–	–	+
15	DSDP Site 400A	Meriadzek Escarpment	–	–	+
16	DSDP Site 512	Falkland Plateau	+	–	–
17	DSDP Site 513	Mid-Atlantic Ridge	+	–	–
18	DSDP Site 613	New Jersey continental rise	–	–	+
19	ODP Site 660	Kane Gap	–	+	–
20	ODP Site 748	Southern Kerguelen Plateau	–	+	–
21	ODP Site 753	Broken Ridge	–	–	+
22	ODP Site 913	East Greenland Basin	–	–	+
23	ODP Site 1050	Blake Nose	+	–	–
24	ODP Site 1051	Blake Nose	–	+	–
25	ODP Site 1172	East Tasman Plateau	–	–	+
26	ODP Site 1218	central Equatorial Pacific Ocean	–	–	+
27	ODP Site 1260	Demerara Rise	–	–	+
28	Islas Orcadas Cruise 1678, Core 46	Falkland Plateau	+	–	–
	Neritic and onshore sites:				
29	Mt Diablo Area	California, USA	+	–	+
30	Barbados	Barbados	–	+	–
31	Kharkov and Luhansk Districts	Ukraine	–	–	+
32	Bolshoi Aktai River	Sverdlovsk District, Russia	+	–	+
33	Aktobe Region	Kazakhstan	–	–	+
34	Turgai Basin	Kazakhstan	–	–	+
35	Ayakkuduk Region	Uzbekistan	–	–	+
36	Ol'ga and Kronotskii canyons	Kamchatka Peninsula, Russia	–	–	+
37	Il'pinskii Peninsula	Kamchatka Peninsula, Russia	–	–	+
38	McMurdo Sound	East Antarctica	–	–	+

Table 1. List of diatom records examined and referenced in the present study. For a comprehensive list of materials used, see the Appendix. Site numbers given in column '#' correspond to site numbers in Text-figs 1, 5 and 8, and Table 3

Microscopy

SEM examination of specimens for this study was performed at several institutions, including: Faculty of Biological Sciences, Johann-Wolfgang-Göthe Universität, Frankfurt am Main (Hitachi S800 microscope); Faculty of Materials Science and Engineering, Warsaw University of Technology (Hitachi S5500 and SU8000 microscopes); and Faculty of Geology, University of Warsaw (JEOL JSM-6380LA microscope).

At SZCZ, LM examination and photography were performed by means of a Leica DMLB microscope fitted with a Nikon DigitalSight camera. Specimens were photographed under a ×50 oil immersion objective. At BM, slides were examined by means of a Zeiss Axioscope.A1 microscope equipped with a Zeiss mRC digital camera. In order to avoid damage to historic slides, a dry ×40 objective was used for photography. Measurements were carried out on images using Adobe Photoshop CS3 Extended software.

Events/tiepoints	ODP Site 1260 (9°N)			ODP Site 1051 (30.05°N)			DSDP Site 338 (67.79°N)		Age (Ma, GTS2012)
	Depth (rmcd)	±	References	Depth (mcd)	±	References	Depth (mbsf)	References	
T *Areosphaeridium dyktyoplokum*	–	–	–	–	–	–	253.84	Eldrett *et al.* (2004); Egger *et al.* (2016)	33.3–33.5
B *Chiropteridium galea*	–	–	–	–	–	–	253.84	Eldrett *et al.* (2004); Egger *et al.* (2016)	33.1–33.5
Orbital tuning tiepoint 1	49.38	–	Westerhold and Röhl (2013)	–	–	–	–	–	40.37
Orbital tuning tiepoint 2	49.78	–	Westerhold and Röhl (2013)	–	–	–	–	–	40.39
Orbital tuning tiepoint 3	118.45	–	Westerhold and Röhl (2013)	–	–	–	–	–	43.241
Orbital tuning tiepoint 4	119.03	–	Westerhold and Röhl (2013)	–	–	–	–	–	43.26
B C18n.1r	–	–	–	67.53	0.01	Edgar *et al.* (2010)	–	–	39.698
B C18n.2n	–	–	–	89.45	0.55	Edgar *et al.* (2010)	–	–	40.145
B C18r	65.51	1.73	Suganuma and Ogg (2006)	138.42	0.01	Edgar *et al.* (2010)	–	–	41.154
B C19n	68.45	1.21	Suganuma and Ogg (2006)	143.53	0.01	Edgar *et al.* (2010)	–	–	41.39
B C19r	91.17	1.34	Suganuma and Ogg (2006)	175.43	0.35	Ogg and Bardot (2001)	~280	Eldrett *et al.* (2004)	42.301
B C20n	125.285	2.22	Suganuma and Ogg (2006)	256.245	1.275	Ogg and Bardot (2001)	–	–	43.432
B C20r	174.65	0.50	Suganuma and Ogg (2006)	366.635	2.045	Ogg and Bardot (2001)			45.724
B C21n	209.045	3.16	Suganuma and Ogg (2006)	395.925	2.075	Ogg and Bardot (2001)			47.349
B C23n	–	–	–	412.795	1.835	Luciani *et al.* (2016)	–	–	51.833

Table 2. Age model tie points for DSDP Site 338, and ODP Sites 1051 and 1260. Abbreviations: B − base of taxon range/magnetozone; T − top of taxon range; rmcd − revised metres composite depth; mcd − metres composite depth; mbsf − metres below sea floor

TERMINOLOGY

General diatom terminology follows Anonymous (1975) and Ross *et al.* (1979). The term "projection" is used following Ross and Sims (1985, p. 285, defined as 'distal parts of the valves […] distinguishable as entities'). In biostratigraphic considerations, B (bottom) and T (top) are used for lowest/first occurrences and highest/last occurrences, respectively, following the convention used in Gradstein *et al.* (2012) and Agnini *et al.* (2014).

RESULTS

Systematic palaeontology

Family Biddulphiaceae Kützing 1844
Genus *Fenneria* J. Witkowski, gen. nov.
(Generitype *Fenneria brachiata* (Brightwell, 1856) J. Witkowski, comb. nov.)

DESCRIPTION: Frustules rectangular in girdle view, valves tri- or quadripolar, solitary or united in short chains. Valve face flat or slightly undulate, with poles either level with the central area, or slightly raised. Mantle generally perpendicular to the valve face, and of variable depth. Valves poroid, with large, scattered areolae on the valve face. Small granules and/or spinules often present between areolae on the valve face. Mantle areolae often finer than on the valve face, aligned in rows parallel to the pervalvar axis. Mantle margin serrated. Hyaline costae present on the valve interior, not involved in valvocopula attachment, sometimes strongly expanded distally. Girdle bands closed, poroid. Rimoportulae inconspicuous, usually placed on the central area next to internal costae.

HABITAT: Fossil marine, planktic.

DERIVATION OF NAME: This genus is named for Dr. Juliane M. Fenner, formerly of Bundesanstalt für Geowissenschaften und Rohstoffe (Federal Institute for Geosciences and Natural Resources), Hannover, Germany, in recognition of her expertise in Palaeogene diatom taxonomy and biostratigraphy.

Fenneria brachiata (Brightwell, 1856) J. Witkowski, comb. nov.

(SEM: Pl. 1, Figs 1−10; LM: Pl. 2, Figs 1−31)

BASIONYM:

1856. *Triceratium brachiatum* n. sp.; Brightwell, p. 274, pl. 17, figs 3, 3x, 3xx.

SYNONYMS:

1861b. *Triceratium inconspicuum* n. sp.; Greville, p. 70, pl. 8, fig. 10.
1876. *Triceratium brachiatum* Brightwell; Schmidt, pl. 77, figs 22, 24.
1876. *Triceratium inconspicuum* Greville; Schmidt, pl. 77, figs 25−28.
1894. *Amphitetras inconspicua* (Greville) De Toni n. comb.; De Toni, p. 905.
1949 *Triceratium brachiatum* Brightwell; Proschkina-Lavrenko, p. 167, pl. 62, figs 8a, 8b.
1949. *Triceratium inconspicuum* Greville; Proschkina-Lavrenko, p. 166, pl. 62, fig. 6.
1957 *Triceratium barbadense* Greville; Kanaya, p. 100, pl. 7, figs 1−4.
1957. '*Triceratium* (*Amphitetras*) *inconspicuum*'; Kanaya, p. 103, pl. 7, fig. 8.
1969. '*Triceratium barbadensis* Grev.'; Gleser, p. 70, pl. 5, fig. 8.
1974. *Triceratium brachiatum* Brightwell; Gleser and Jousé, p. 58, text-figs 3.3−3.7.
1974. *Triceratium barbadense* Greville; Gleser *et al*., pl. 32, fig. 9; pl. 36, fig. 2.
1977. *Triceratium barbadense* Greville; Fenner, p. 534, pl. 30, figs 12−14.
1977. *Triceratium inconspicuum* var. ('*trilobata*') *trilobatum* n. var.; Fenner, p. 534, pl. 30, figs 23−26.
1978. *Triceratium barbadense* Greville; Dzinoridze *et al.*, pl. 10, fig. 1.
part 1979. *Triceratium barbadense* Greville; Dzinoridze *et al.*, p. 52, text-figs 144−149, non text-fig. 150.
1984. *Triceratium inconspicuum* var. *trilobata* Fenner; Barron *et al.*, p. 158, pl. 6, figs 6, 7.
1985. *Triceratium brachiatum* Brightwell; Fenner, text-figs 8.19−8.23.

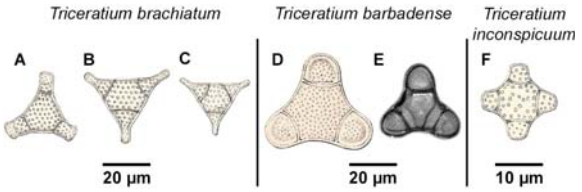

Text-fig. 2. Reproductions of original line drawings of *Triceratium brachiatum* Brightwell, 1856 (**A**-**C**), *Triceratium barbadense* Greville, 1861a (**D**), along with a photomicrograph of a specimen from the type slide (**E**), and *Triceratium inconspicuum* Greville, 1861b (**F**). A − original of Brightwell (1856, pl. 17, fig. 3); B − original of Brightwell (1856, pl. 17, fig. 3x); C − original of Brightwell (1856, pl. 17, fig. 3xx); D − original of Greville (1861a, pl. 4, fig. 12); E − LM of a slightly tilted valve resembling *T. barbadense* on type slide BM2079; F − original of Greville (1861b, pl. 8, fig. 10)

1985. '*Triceratium inconspicuum* Greville var. *inconspicuum*'; Fenner, p. 740, text-figs 8.17, 8.18.
1985. *Triceratium inconspicuum* var. *trilobata* Fenner; Fenner, p. 740, text-figs 8.12−8.16.
1986. *Lisitzinia inconspicua* (Greville) Gleser n. comb.; Gleser *et al*., p. 858, pl. 1, figs 4a, 4b.
1996. *Triceratium inconspicuum* Greville; Scherer and Koç, p. 89, pl. 8, fig. 4.
2000. *Triceratium inconspicuum* var. *trilobata* Fenner; Harwood and Bohaty, p. 94, pl. 4, fig. L.
2002. *Lisitzinia inconspicua* (Greville) Gleser; Olshtynskaya, p. 122, pl. 2, figs 7, 8; pl. 3, figs 1, 2.
2003. '*Lisitzinia brachiatum* (Brightwell) Gleser'; Tsoy, p. 381, pl. 2, fig. 6. [nomen nudum]
2003. '*Lisitzinia inconspicua* (Greville) Gleser var. *trilobata* Gleser'; Tsoy, p. 381, figs 2a, b.
2011. *Triceratium brachiatum* Brightwell; Paier, p. 76, text-fig. 4L.
non 2011. *Triceratium inconspicuum* var. *trilobata* Fenner; Paier, p. 76, text-fig. 3Y−3BB [= *F. kanayae*, see below].
non 2012. *Triceratium inconspicuum* Greville; Manchester *et al.*, text-figs 4−12.
2012a. *Triceratium inconspicuum* var. *trilobata* Fenner; Witkowski *et al.*, pl. 4, figs 4a, 4b.
2013. *Triceratium inconspicuum* var. *trilobata* Fenner; Gladenkov, p. 75, text-figs 3.3, 3.4.
2014. '*Triceratium inconspicuum* Greville var. *inconspicuum*'; Witkowski *et al.*, pl. 1, fig. 14.
2014. *Triceratium inconspicuum* var. *trilobata* Fenner; Witkowski *et al.*, pl. 1, fig. 15.

NEOTYPE: BM 2084, Greville Collection, 'Barbadoes earth' (Pl. 2, Fig. 4).

DESCRIPTION: Frustules rectangular to subrectan-

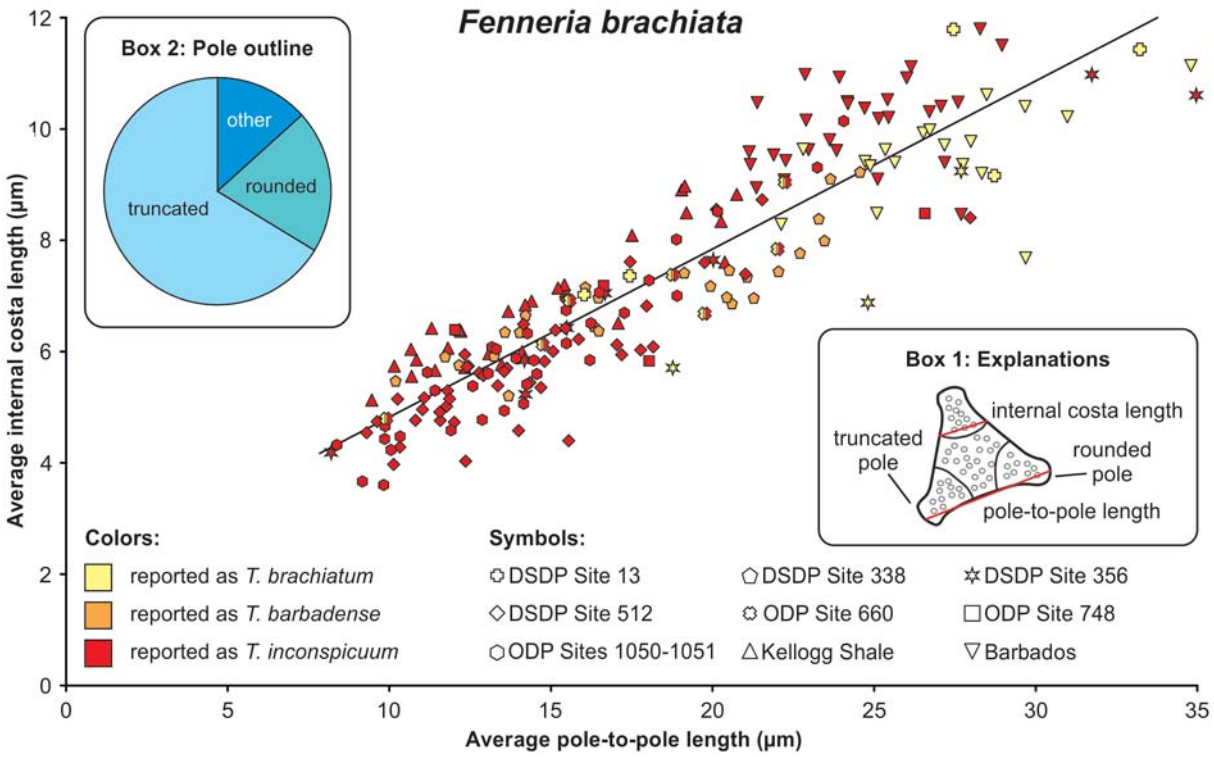

Text-fig. 3. Morphometry of *Fenneria brachiata* (Brightwell) J. Witkowski, comb. nov. showing average pole-to-pole length plotted versus average internal costa length (see Box 1 for measurement explanation). Box 2 shows the percentage of valves with truncated, rounded, and other types of pole outline among the measured specimens

gular in girdle view (Pl. 1, Fig. 1), valves tri- to quadripolar (Pl. 1, Figs 3−8; Pl. 2, Figs 1−30). Valve face flat or gently undulate (Pl. 1, Figs 1, 5; Pl. 2, Fig. 31). Undulate valves usually have a small, slightly convex, dome-shaped central area, and slightly raised poles with flat summits (Pl. 1, Figs 1, 2). Some valves have a gently depressed central area (Pl. 1, Fig. 5). Valve outline is highly variable, especially with respect to the shape and length of the projections, whose terminations can be rounded (e.g., Pl. 2, Fig. 3), truncated (e.g., Pl. 2, Fig. 9), or even slightly produced (e.g., Pl. 2, Fig. 1). Mantle shallow (Pl. 1, Fig. 1; Pl. 2, Fig. 31), clearly separated from the valve face, with a serrated margin (Pl. 1, Figs 6−8; Pl. 2, Fig. 31). Areolae on the valve face are scattered, large (Pl. 1, Figs 3, 6). Granules and/or spinules are commonly scattered in between areolae on the valve face (Pl. 1, Fig. 1). Mantle areolae aligned in short rows parallel to the pervalvar axis (Pl. 1, Fig. 1; Pl. 2, Fig 31). Internally, the mantle margin is slightly expanded toward the valve interior (Pl. 1, Figs 6−8). Each projection is separated from the central area by an arching internal costa (Pl. 1, Figs 6, 7). Small rimoportulae, located on the central area next to the internal costae (Pl. 1, Figs 9, 10), open both to the valve exterior and interior as short tubes.

MEASUREMENTS (based on tripolar valves; n = 200; Text-fig. 3): average pole-to-pole length: 17.7 µm; average internal costa length: 7.2 µm; average areolation density: 6 in 10 µm; number of rimoportulae: 2.

DISCUSSION: Although it is one of the most common Eocene diatoms worldwide, *F. brachiata* is surrounded by a considerable taxonomic confusion, with several synonyms used interchangeably even in various works of the same authors, and with numerous orthographic variants. The multitude of names, under which this species is commonly referred to in the literature, however, can be traced to three taxa: *T. barbadense*, *T. brachiatum* and *T. inconspicuum*. *Triceratium brachiatum* is given priority for reasons discussed below.

The description of *T. brachiatum* given by Brightwell (1856) is based on material labelled as "Barbadoes earth", and accompanied by three line drawings that suggest broad limits of morphological variation for this species (reproduced here in Text-

fig. 2A–C). All specimens illustrated by Brightwell (1856) display different valve outlines, especially with respect to length and breadth of the projections. Unfortunately, it is impossible to re-examine Brightwell's type specimens, as no slides of the Barbados materials are reported as extant in what remains of Brightwell's collection (Clarke 1986). Notably, however, the figures indicate that Brightwell (1856) considered both forms with truncated poles and forms with rounded poles as part of the range of variation of *T. brachiatum*. Subsequent workers (e.g., Fenner 1985) used the shape of projections to distinguish between *T. brachiatum* (as having tapering projections) and *T. inconspicuum*. This issue is further discussed below.

The confusion between *T. barbadense* on the one hand, and *T. brachiatum* and *T. inconspicuum* on the other, is more puzzling. *Triceratium inconspicuum* is discussed twice in Greville's works (Greville 1861a, b). However, both the brief mention in Greville (1861a) and the proper description in Greville (1861b) emphasize that Greville's specimens from Barbados were quadripolar. Greville (1861b) also remarked on the high morphological similarity between *T. inconspicuum* and *T. brachiatum*, but emphasized the difference in valve diameter between the two species. Indeed, Greville's (1861b, pl. 8, fig. 10) illustration of *T. inconspicuum* shows a valve that is approximately half the size of the specimens that Brightwell (1856) illustrated as *T. brachiatum* (see Text-fig. 2A–C versus Text-fig. 2F). Despite the difference in size and number of poles, however, the overall morphology of *T. inconspicuum* is remarkably similar to that of *T. brachiatum*.

Williams (1988) designated slide BM 2084 as the type for *T. inconspicuum* and provided a microphotograph of the holotype, a quadripolar valve (Williams 1988, pl. 63, figs 2, 3). Careful examination of the entire type slide performed as part of this study, however, showed an abundance of tripolar valves (Pl. 2, Figs 4, 7), but failed to locate a quadrate specimen. As Greville (1861b) made no mention of the morphological variation within *T. inconspicuum*, it appears that subsequent workers must have restricted *T. inconspicuum* to quadrate forms. Thus, tripolar valves of similar diameter and morphology were identified either as *T. brachiatum* or *T. barbadense*. However, Greville's (1861a) description of the latter, based also on the material from Barbados, indicates that it is morphologically similar to *Triceratium castellatum* West, 1860. This is corroborated by Greville's illustration of *T. barbadense* (Greville 1861a, pl. 4, fig. 12; reproduced here in Text-fig. 2D), showing a specimen with a valve outline that does not fit within the range of variation observed either for *T. inconspicuum* or *T. brachiatum*.

Slide BM 2079, indicated by Williams (1988) as one of two type slides for *T. barbadense*, was examined in the present study to verify whether *T. barbadense* and *T. brachiatum* or *T. inconspicuum* are conspecific. Indeed, co-occurring with numerous tripolar specimens of *T. inconspicuum* or *T. brachiatum*, a slightly tilted valve of a diatom remarkably similar to *T. castellatum* was found on slide BM 2079 (see Text-fig. 2E). Unfortunately, the second type slide for *T. barbadense* (BM 2049) is destroyed, and Williams (1988) provided no photomicrographs of the type specimen of *T. barbadense*.

As can be seen from the above discussion, it seems clear why subsequent workers used *T. brachiatum* and *T. inconspicuum* interchangeably, and why some workers distinguished between the two species (e.g., Proschkina-Lavrenko 1949; Fenner 1985; Radionova 1996; Renaudie *et al.* 2010). It remains a puzzle, however, how and why *T. barbadense* came to be treated as a synonym of *T. brachiatum* or *T. inconspicuum*. The morphology of *T. castellatum*, subsequently transferred as *Sheshukovia castellata* (West) Gleser, 1975, is distinctly different from *T. brachiatum* and *T. inconspicuum* as evident even in LM examination.

Fenner (1977) was the first to formally distinguish between tri- and quadripolar variants of *T. inconspicuum*. She followed Greville (1861a, b) in that *T. inconspicuum* was originally described as a quadrate species. The more common tripolar variant was named var. *trilobata*. Fenner's tripolar variety later served as the basionym for the new combination of Gleser *et al.* (1986), who transferred *T. inconspicuum* to *Lisitzinia* Jousé, 1978 as *L. inconspicua* var. *trilobata* (Fenner) Gleser in Gleser *et al.*, 1986. The quadrate variety was transferred as *L. inconspicua* (Greville) Gleser in Gleser *et al.*, 1986. Tsoy (2003), apparently following Gleser *et al.* (1986), cited '*Lisitzinia brachiata* (Brightwell) Gleser'; as no such combination was published by Gleser, it is here considered as *nomen nudum*. Three other names are found in the literature that reflect the uncertainty as to the proper generic placement of *T. brachiatum* and *T. inconspicuum*. Kanaya (1957), following De Toni (1894), reported this species as '*Triceratium* (*Amphitetras*) *inconspicuum*', Scherer *et al.* (2007) – as '*Triceratium* (*Lisitzinia*) *inconspicuum*' , and Barron *et al.* (2014) – as '*Triceratium* (*Sheshukovia*) *inconspicuum*'. Morphologically, however, *T. brachiatum* and *T. inconspicuum* differ considerably from the generitypes of both *Amphitetras* Ehrenberg,

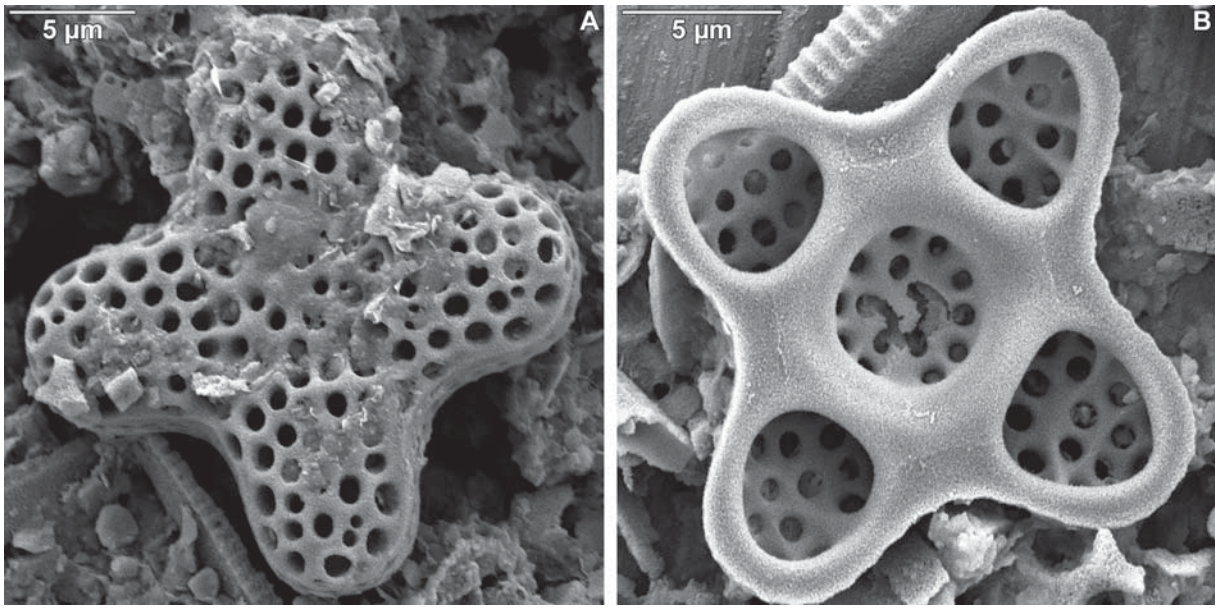

Text-fig. 4. Scanning electron micrographs showing valve morphology of *Lisitzinia ornata* Jousé, 1978 from SZCZ 15068 (see the Appendix). A − Oblique external view; B − Internal view. Note absence of rimoportulae and smooth mantle margin

1840 (Ross and Sims 1971; Ashworth *et al.* 2013) and *Sheshukovia* Gleser, 1975 (see Witkowski *et al.* 2015). Apparently, neither *T. brachiatum* or *T. inconspicuum* belong to *Amphitetras* or *Sheshukovia*.

In order to examine Gleser's taxonomic perspective on *T. inconspicuum*, valves of *Lisitzinia ornata* Jousé, 1978, the generitype of *Lisitzinia*, were examined in SEM (Text-fig. 4). A considerable difference in valve structure can be observed between *T. inconspicuum* and *L. ornata*. Valves of *L. ornata* have a greatly reduced mantle depth and an entirely smooth mantle margin (Text-fig. 4B). Areolae on the valve face of *L. ornata* are arranged in well-defined rows, parallel to both axes of the cruciform valve (Text-fig. 4A). No tripolar valves of *L. ornata* are reported in the literature, and the only species that appears to closely resemble *L. ornata* in valve morphology is *Triceratium blanditum* Greville, 1861b. This, however, has never been examined in SEM (for LM examination of the holotype see Williams 1988, pl. 59, fig. 4). There is also considerable stratigraphic difference between the occurrence of *T. inconspicuum*, largely restricted to the lower to middle Eocene, and *Lisitzinia*, which is an important zonal marker for the upper Oligocene in the Southern Ocean (Roberts *et al*. 2003; Scherer *et al*. 2007). Thus, *T. inconspicuum* should not be placed in *Lisitzinia*.

Finally, morphometric analysis was employed to further explore whether *T. brachiatum* and *T. inconspicuum* are conspecific (Text-fig. 3). Specimens from several slides from the BM collections labelled as *Triceratium brachiatum*, and all tripolar specimens found on Greville's type slide for *T. inconspicuum* (BM 2084) were examined and measured in LM for this study (Table A2 in the Appendix). Valves from a number of localities worldwide were also examined and measured in LM (Text-fig. 3). Additionally, specimens illustrated by Brightwell (1856), as well as those illustrated as *T. brachiatum* by Gleser and Jousé (1974) and Fenner (1985), were measured for comparison. Regardless of the identification, specimens from all localities plot together showing a pronounced linear trend (Text-fig. 3). Specimens from BM slides and valves illustrated by Brightwell (1856) tend to cluster in the upper pole-to-pole length range. This may represent a bias introduced by sieving of the residues, from which specimens were selected for mounting. On the contrary, most specimens from unsieved slides from deep-sea cores cluster together in the lower pole-to-pole length range. As some workers used the pole outline to distinguish between *T. brachiatum* and *T. inconspicuum*, all measured specimens were also inspected for the shape of the poles (Box 2 in Text-fig. 3). Valves with truncated poles were more common than those with rounded poles. Notably, however, some specimens showed both types of pole outline (Pl. 2, Fig. 18; Box 2 in Text-fig. 3). Overall, given the morphometric evidence, the

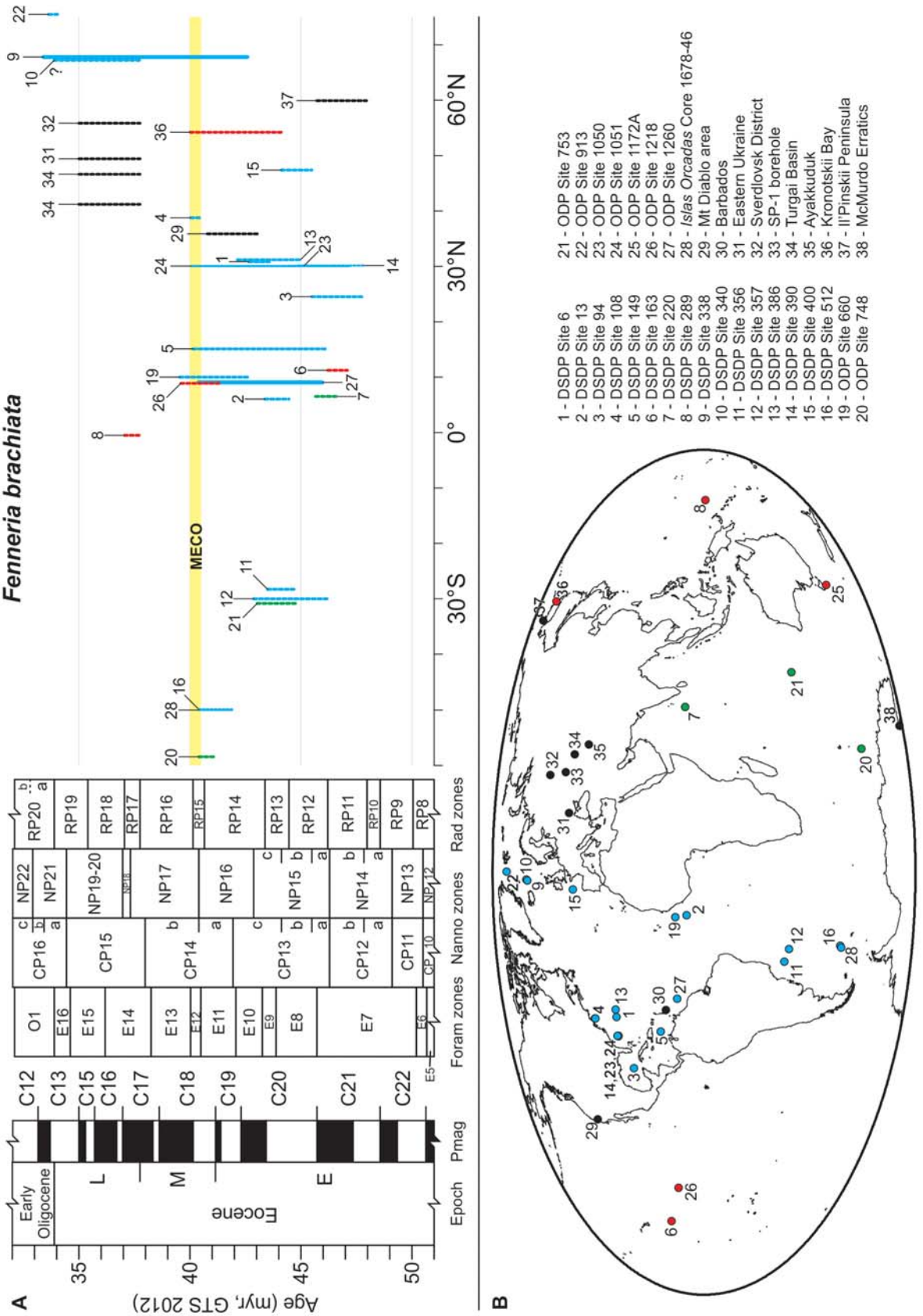
A
Fenneria brachiata
MECO
Age (myr, GTS 2012)
Epoch
Pmag
Foram zones
Nanno zones
Rad zones
Early Oligocene
Eocene
L
M
E
C12
C13
C15
C16
C17
C18
C19
C20
C21
C22
O1
E16
E15
E14
E13
E12
E11
E10
E9
E8
E7
E6
E5
CP16
CP15
CP14
CP13
CP12
CP11
CP10
NP22
NP21
NP19-20
NP18
NP17
NP16
NP15
NP14
NP13
NP12
RP20
RP19
RP18
RP17
RP16
RP15
RP14
RP13
RP12
RP11
RP10
RP9
RP8
60°N
30°N
0°
30°S
B
1 - DSDP Site 6
2 - DSDP Site 13
3 - DSDP Site 94
4 - DSDP Site 108
5 - DSDP Site 149
6 - DSDP Site 163
7 - DSDP Site 220
8 - DSDP Site 289
9 - DSDP Site 338
10 - DSDP Site 340
11 - DSDP Site 356
12 - DSDP Site 357
13 - DSDP Site 386
14 - DSDP Site 390
15 - DSDP Site 400
16 - DSDP Site 512
19 - ODP Site 660
20 - ODP Site 748
21 - ODP Site 753
22 - ODP Site 913
23 - ODP Site 1050
24 - ODP Site 1051
25 - ODP Site 1172A
26 - ODP Site 1218
27 - ODP Site 1260
28 - Islas Orcadas Core 1678-46
29 - Mt Diablo area
30 - Barbados
31 - Eastern Ukraine
32 - Sverdlovsk District
33 - SP-1 borehole
34 - Turgai Basin
35 - Ayakkuduk
36 - Kronotskii Bay
37 - Il'Pinskii Peninsula
38 - McMurdo Erratics

separation between *T. brachiatum* and *T. inconspicuum* is not justified. As a senior binomial, *T. brachiatum* has priority over *T. inconspicuum* and is transferred here into the new genus *Fenneria* as *Fenneria brachiata*. However, since at present no type can be designated from Brightwell's materials, the specimen on slide BM 2084 figured in Pl. 2, Fig. 4 is proposed as the neotype.

GEOGRAPHIC AND STRATIGRAPHIC DISTRIBUTION (Text-fig. 5; for data and references see Table 3): *Fenneria brachiata* occurs both at pelagic sites (e.g., DSDP Sites 6 and 163) and in coastal settings (e.g., the Kellogg Shale, Ukrainian localities), which suggests a planktic mode of life. Although most records come from the low- and mid-latitude Atlantic Ocean, *F. brachiata* occurs *in situ* from ~60º S to ~75º N. The report from the McMurdo Erratics found at ~76º S, although glacially displaced, indicates the presence of *F. brachiata* also in the southern high latitudes. This species has a global distribution, consistent with the interpretation as a planktic diatom.

The mid- and high southern latitude occurrences of *F. brachiata* are restricted to the late early and earliest middle Eocene (Text-fig. 5). However, most of the available records span narrow stratigraphic intervals (e.g., DSDP Site 512, ODP Site 748), or are not well constrained stratigraphically (e.g., the diatom-bearing intervals at DSDP Site 357 and ODP Site 753). Regardless, none of the Southern Hemisphere records show the presence of *F. brachiata* after the Middle Eocene Climatic Optimum event (MECO – see Bohaty *et al*. 2009; Witkowski *et al.* 2014; Text-fig. 5; Table 3).

Tropical and mid-northern latitude records indicate a slightly longer stratigraphic range for *F. brachiata* than Southern Hemisphere sites. ODP Sites 1260 and 1051, in the tropical and mid-latitude Atlantic, respectively, offer long records of diatom evolution with excellent age control, and are discussed in more detail below. The stratigraphic range of *F. brachiata* as determined at Site 1051 is consistent with observations from DSDP Sites 6, 108 and 386, all located in the western North Atlantic, and from the Kellogg Shale in California (Text-fig. 5; Table 3). DSDP Sites 94 and 390 appear to record B *F. brachiata* somewhat earlier than at Site 1051 (Text-fig. 5). This is because Fenner (1984a) did not specify the depth range of *F. brachiata* at Sites 94 and 390. Except for one record (DSDP Site 289), which may represent a misidentification or reworking, all onshore and deep-sea low-and mid-northern latitude records show a middle early to early middle Eocene range for *F. brachiata*. ODP Site 1218, which has a robust biomagnetostratigraphic age control, is the only low- to mid-latitude record showing the occurrence of *F. brachiata* after the termination of the MECO event (Text-fig. 5; Table 3). This may indicate a diachronous upper range for the *F. brachiata* occurrences between the tropical Atlantic and the tropical Pacific regions.

Northern high latitude records of *F. brachiata* show a broad scatter of stratigraphic ranges, which is in part due to limited age control. Onshore occurrences in the numerous eastern Ukrainian localities, as well as within the Turgai Basin (Kazakhstan) and Sverdlovsk District (Russia), lack refined age control and are usually reported as late Eocene (Text-fig. 5; Table 3). The early Oligocene age of the occurrence in the Sverdlovsk District (Proschkina-Lavrenko 1949) is questioned here and thus not included in this compilation, pending a revised dating of these sediments. Despite the excellent preservation, the diatom-bearing sequences of the Eurasian platform often lack calcareous microfossils and require correlation via organic-walled zonal markers (e.g., Oreshkina *et al*. 2004). The Il'pinskii Peninsula occurrence (Kamchatka, Russia) is based on a single sample. Other high-northern latitude records (e.g., Ol'ga and Kronotskii canyons, Kamchatka, Russia, and DSDP Site 338), however, are well-constrained, and indicate a considerably longer stratigraphic range for *F. brachiata* than in both southern and low- and mid-northern latitude regions. Taken together, the records from Kamchatka and DSDP Site 338 indicate the presence of *F. brachiata* from the middle/late early Eocene to the early Oligocene (Text-fig. 5; Table 3).

← Text-fig. 5. Stratigraphic and geographic distribution of *Fenneria brachiata* (Brightwell) J. Witkowski, comb. nov. Numbers denote individual deposits, as listed in the lower right corner. Chronostratigraphy, magnetostratigraphy, and foraminiferal and nannofossil zonations following Gradstein *et al.* (2012); radiolarian zonation following Norris *et al.* (2014). A − Stratigraphic distribution of *F. brachiata* in datable deposits considered in this study plotted versus latitude. For essential stratigraphic information on the deposits included in this compilation see the Appendix and Table 3. Blue – Atlantic sites; green – Indian Ocean sites; red – Pacific sites; black – neritic and onshore sites. Dashed lines indicate approximate stratigraphic ranges. Solid lines indicate well-constrained stratigraphic ranges; B − Geographic distribution of *F. brachiata.* Site numbers correspond to numbers given in Text-figs 1 and 8, and Table 3 (column '#'). Base map plotted using Ocean Drilling Stratigraphic Network advanced plate tectonic reconstruction application (www.odsn.de)

#	Locality	*Fenneria brachiata*				*Fenneria kanayae*				References
		lowest level present	correlation	highest level present	correlation	lowest level present	correlation	highest level present	correlation	
1	DSDP Site 6	229.8 mbsf	E10	192.3 mbsf	E9	229.8 mbsf	E10	192.3 mbsf	E9	this study
2	DSDP Site 13	145.0 mbsf	RP13	136.0 mbsf	RP13	–	–	–	–	Fenner (1985)
3	DSDP Site 94	depth unspecified	mid-NP14	depth unspecified	lower NP15	depth unspecified	mid-NP14	depth unspecified	lower NP15	Fenner (1984a, 1985)
4	DSDP Site 108	44.8 mbsf	E12	44.8	E12	–	–	–	–	Fenner (1985)
5	DSDP Site 149	~380 mbsf	lower RP12	depth unspecified	RP15/RP16 transition	~380 mbsf	lower RP12	depth unspecified	RP13/RP14 transition	Fenner (1984a)
6	DSDP Site 163	82.74 mbsf	upper RP11	82.74 mbsf	upper RP11	–	–	–	–	Fenner (1984b)
7	DSDP Site 220	260.21 mbsf	upper RP11	254.21 mbsf	lower RP12	260.21 mbsf	upper RP11	237.67 mbsf	RP12	Fenner (1984b)
8	DSDP Site 289	1004.05 mbsf	RP17	1004.05 mbsf	RP17	–	–	–	–	Fenner (1984b)
9	DSDP Site 338	278.97 mbsf	upper C20n?	249.59 mbsf	C12r? C13n?	–	–	–	–	Schrader and Fenner (1976); Dzinoridze *et al.* (1978, 1979); Eldrett *et al*. (2004)
10	DSDP Site 340	101.7 mbsf	middle/ upper Eocene	11.6 mbsf	middle/ upper Eocene	–	–	–	–	Schrader and Fenner (1976)
11	DSDP Site 356	191.8 mbsf	NP15b	115.8 mbsf	NP15c	191.8 mbsf	NP15b	115.8 mbsf	NP15c	Fenner (1977)
12	DSDP Site 357	358.6	NP15	356.58	NP15	–	–	–	–	Fenner (1984b)
13	DSDP Site 386	385.77 mbsf	NP15b	330.42 mbsf	NP16	385.77 mbsf	NP15b	330.42 mbsf	NP16	this study
14	DSDP Hole 390A	51.8 mbsf	mid-NP14	depth unspecified	NP15	51.8 mbsf	mid-NP14	depth unspecified	NP15	Fenner (1984a)
15	DSDP Hole 400A	~540 mbsf	NP15b	~535 mbsf	NP15b	~570 mbsf	basal NP14	~555 mbsf	mid-NP15b	Radionova (1996)
16	DSDP Site 512	75.8 mbsf	CP14a	20.66 mbsf	CP14a	–	–	–	–	Gombos (1983)
18	DSDP Site 613	–	–	–	–	290.2 mbsf	upper RP12	280.6 mbsf	upper RP12	Abbott (1987)
19	ODP Site 660	144 mbsf	RP14	118.3 mbsf	RP16	118.3 mbsf	RP16	118.3 mbsf	RP16	Baldauf and Pokras (1989)
20	ODP Site 748	170.75 mbsf	upper CP14a	159.67 mbsf	upper CP14a	170.91 mbsf	upper CP14a	164.67 mbsf	upper CP14a	Witkowski *et al*. (2012b)
21	ODP Site 753	55.75 mbsf	CP13c	55.75 mbsf	CP13c	depth unspecified	CP13b	depth unspecified	CP13b	Peirce *et al*. (1988)
22	ODP Site 913	497.5 mbsf	C18n	497.5 mbsf	C18n	–	–	–	–	Scherer and Koç (1996); Eldrett *et al*. (2004)
23	ODP Site 1050	112.9 mbsf (Hole B)	CP13b	112.9 mbsf (Hole B)	CP13b	85.94 mbsf (Hole A)	CP13b	85.94 mbsf (Hole A)	CP13b	this study
24	ODP Site 1051	388.29 mcd	lower C21n	84.22 mcd	C18n.2n	388.29 mcd	lower C21n	273.49 mcd	upper C20r	Witkowski *et al*. (2014); this study
25	ODP Hole 1172A	depth unspecified	–	depth unspecified	–	–	–	–	–	Stickley *et al.* (2004b)

#	Locality	*Fenneria brachiata*				*Fenneria kanayae*				References
		lowest level present	correlation	highest level present	correlation	lowest level present	correlation	highest level present	correlation	
26	ODP Site 1218	291.53 mcd	upper CP14a	271.93 mcd	lower CP14b	–	–	–	–	Bohaty (unpublished)
27	ODP Site 1260	178.9 rmcd	upper C21n	56.04 rmcd	C18r	178.9 rmcd	upper C21n	120.52 rmcd	lower C20n	Suganuma and Ogg (2006); Renaudie *et al*. (2010); Westerhold and Röhl (2013)
28	Islas Orcadas Core 1678-46	0.24 mbsf	middle Eocene	0.22 mbsf	middle Eocene	0.24 mbsf	middle Eocene	0.22 mbsf	middle Eocene	Gombos (1982b); this study
29	Kellogg Shale	0 m	upper CP13c	23.2 m	topmost CP14a	0	upper CP13c	3.6 m	basal CP14a	Barron *et al*. (1984)
30	Barbados	–	middle Eocene-lower Miocene	–	middle Eocene-lower Miocene	–	–	–	–	Brightwell (1856), Greville (1861b), Schmidt (1876)
31	Eastern Ukraine	–	upper Eocene / lower Oligocene	–	upper Eocene / lower Oligocene	–	–	–	–	Proschkina-Lavrenko (1949); Gleser *et al*. (1965, 1974); Olshtynskaya (2002)
32	Yekaterinburg District	–	upper Eocene	–	upper Eocene	–	–	–	–	Proschkina-Lavrenko (1949)
33	SP-1 borehole, Aktobe region	~105 m	upper NP14	~95 m	upper NP15	~105 m	upper NP14	~55 m	NP16/ NP17 transition	Radionova (1996)
34	Turgai Basin	–	upper Eocene	–	upper Eocene	–	–	–	–	Gleser (1969); Gleser *et al*. (1974)
35	Ayakkuduk region	depth unspecified	upper Eocene	depth unspecified	upper Eocene	–	–	–	–	Shibkova (1968)
36	Kronotskii Bay	depth unspecified	upper NP15	depth unspecified	basal NP17	depth unspecified	mid-NP14	depth unspecified	NP15?	Tsoy (2003)
37	Il'pinskii Peninsula	outcrop depth unspecified	E7a-b	outcrop depth unspecified	E7a-b	–	–	–	–	Gladenkov (2013)
38	McMurdo Erratics	–	middle to upper Eocene	–	middle to upper Eocene	–	–	–	–	Harwood and Bohaty (2000)

Table 3. Geographic and stratigraphic distribution of *Fenneria brachiata* (Brightwell) J. Witkowski, comb. nov. and *Fenneria kanayae* (Fenner) J. Witkowski, comb. nov. Site numbers given in column '#' correspond to site numbers in Text-figs 1, 5 and 8, and Table 1. Abbreviations: rmcd − revised metres composite depth; mcd − metres composite depth; mbsf − metres below sea floor

Fenneria kanayae (Fenner, 1984a) J. Witkowski, comb. nov.

(SEM: Pl. 3, Figs 1−7; LM: Pl. 4, Figs 1−24)

BASIONYM:

1984a. *Triceratium kanayae* n. sp.; Fenner, p. 334, pl. 1, figs 5, 6, pl. 2, figs 3, 4.

SYNONYMS:

1876. '*Triceratium inconspicuum* Grev.?, var.?'; Schmidt, pl. 77, text-fig. 29.

1927. *Trinacria insipiens* Witt; Hanna, p. 123, pl. 21, fig. 7.

1957. '*Triceratium* sp. A'; Kanaya, p. 102, pl. 7, figs 5−7.

1977. *Triceratium schulzii* Jousé; Fenner, p. 535, pl. 30, figs 1−11, pl. 37, fig. 3.

1977. *Triceratium schulzii* Jousé var. *quadriloba* Fenner n. var.; Fenner, p. 535, pl. 30, figs 15–20.
1984. *Triceratium kanayae* Fenner; Barron *et al.*, p. 158, pl. 6, fig. 9.
1984. '*Triceratium kanayae* var. *quadrilobata* Fenner'; Barron *et al.*, p. 158.
1984a. *Triceratium kanayae* var. *kanayae* n. var.; Fenner, p. 334, pl. 1, figs 5, 6.
1984a. *Triceratium kanayae* var. *quadriloba* n. var.; Fenner, p. 334, pl. 2, figs 3, 4.
1986. *Lisitzinia kanayai* (Fenner) Gleser n. comb.; Gleser *et al.*, p. 858, pl. 1, figs 2a, b.
2003. *Lisitzinia kanayai* (Fenner) Gleser; Tsoy, p. 381, pl. 1, figs 1a, 1b.
2011. '*Triceratium inconspicuum* Grev. var. *trilobata*'; Paier, text-figs 3Y–3BB.
2011. *Triceratium kanayae* Fenner; Paier, p. 76, fig. 4M.

HOLOTYPE: Fenner (1984a, pl. 1, fig. 5). Note: the type slide indicated by Fenner (1984a) could not be located in the Hustedt Collection, Bremerhaven (Bank Beszteri, written communication 2017). It proved impossible to determine whether the slide was never donated to the collection, or simply got lost after being reposited.

DESCRIPTION: Frustules rectangular in girdle view (Pl. 4, Fig. 22); valves tripolar (Pl. 3, Figs 1, 2) to quadripolar (Pl. 3, Fig. 4), with a variable outline of poles (Pl. 4, Figs 1–19, 24). Valve face flat, or with slightly raised poles (Pl. 3, Figs 1, 2; Pl. 4, Figs 21, 22). Externally, on the valve poles there are short, shallow furrows separated by low parallel ridges, which serve as cameo/intaglio linking structures (Pl. 3, Fig. 2). Valves perforated by poroid areolae, on the valve face arranged in irregular circles around a prominent central areola or group of areolae. Areolae on the mantle are arranged in weakly defined rows, generally parallel to the pervalvar axis (Pl. 3, Figs 1, 2, 4). Interstrial pores are common both on the valve face and on the mantle (Pl. 3, Fig. 2). Mantle generally perpendicular to the valve face, often gently sloping at the valve face-mantle junction (Pl. 4, Figs 20, 21). Mantle margin coarsely serrate (Pl. 3, Figs 2–5, 7), slightly expanded toward the valve interior (Pl. 4, Fig. 2). In most specimens these inward expansions form prominent pseudosepta at the poles (Pl. 3, Figs 3, 4, 7). On the valve interior, across each polar projection there is a transverse hyaline costa that can be considerably expanded along its distal edge (Pl. 3, Figs 3 and 5 versus Pl. 3, Fig. 4 and Pl. 4, Fig. 24), giving the impression of a sub-rounded polygonal structure surrounding the central area. Within each polar projection, there are also one or two circumferential costae located on the mantle, approximately above the polar pseudoseptum (Pl. 3, Fig. 5; Pl. 4, Figs 21–23). Also on the interior of each projection, in the distal part, there is at least one short radial costa (Pl. 4, Figs 8, 10, 14). These are usually only resolvable in LM. Next to two transverse costae, on the proximal side, there are inconspicuous rimoportulae (Pl. 3, Figs 6, 7). Externally rimoportulae are usually flush with the valve face, and indistinguishable from other openings (Pl. 3, Figs 1, 2), but occasionally can be associated with short external tubes. Rimoportulae open to the valve interior as short tubes (Pl. 3, Figs 6, 7).

MEASUREMENTS (based on tripolar specimens, n = 45; Text-fig. 6): average pole-to-pole length: 26.3 μm; average transverse internal costa length: 10.9 μm; average radial costa length: 3.2 μm; average pseudoseptum depth: 6.5 μm; average areolation density: 5 in 10 μm; number of rimoportulae: 2.

DISCUSSION: Even though it is a zonal marker for a well-established lower Eocene tropical biostratigraphic zone (Fenner 1984a; Scherer *et al*. 2007; Barron *et al*. 2015), *Fenneria kanayae* is not reported as widely as *F. brachiata*. *Fenneria kanayae* also displays a broad range of morphological variation, and small valves have an appearance similar to *F. brachiata* (Text-fig. 6). *Fenneria kanayae* is distinguished by relatively small, but strongly silicified valves with stout projections that bear a short internal, radially oriented costa in the distal part (Pl. 4, Figs 8, 10, 14). The internal placement of the short radial costa, paradoxically, makes identification of *F. kanayae* easier in LM than in SEM. It proved impossible to document the radial costa in SEM in this study, as it is aligned with a pseudoseptum and a series of robust circumferential internal costae that are parallel to the pseudoseptum. All these structures obscure the radial costa in valves viewed from the interior (Pl. 3, Figs 3–7).

The earliest report of a diatom resembling *T. kanayae* is in Schmidt (1876, pl. 77, fig. 29); this single figure is based on the material from Cambridge Estate, Barbados, and labelled as a probable variety of *T. inconspicuum*. It possibly represents a valve with the mantle margin facing toward the viewer. The stout valve outline, vaguely reproduced areolation and radial costae all resemble *F. kanayae*. Hanna's (1927, pl. 21, fig. 7) report on the Eocene Kreyenhagen Shale (California, USA) diatoms includes a high-quality photomicrograph of a diatom that can be confidently identified as *F. kanayae*.

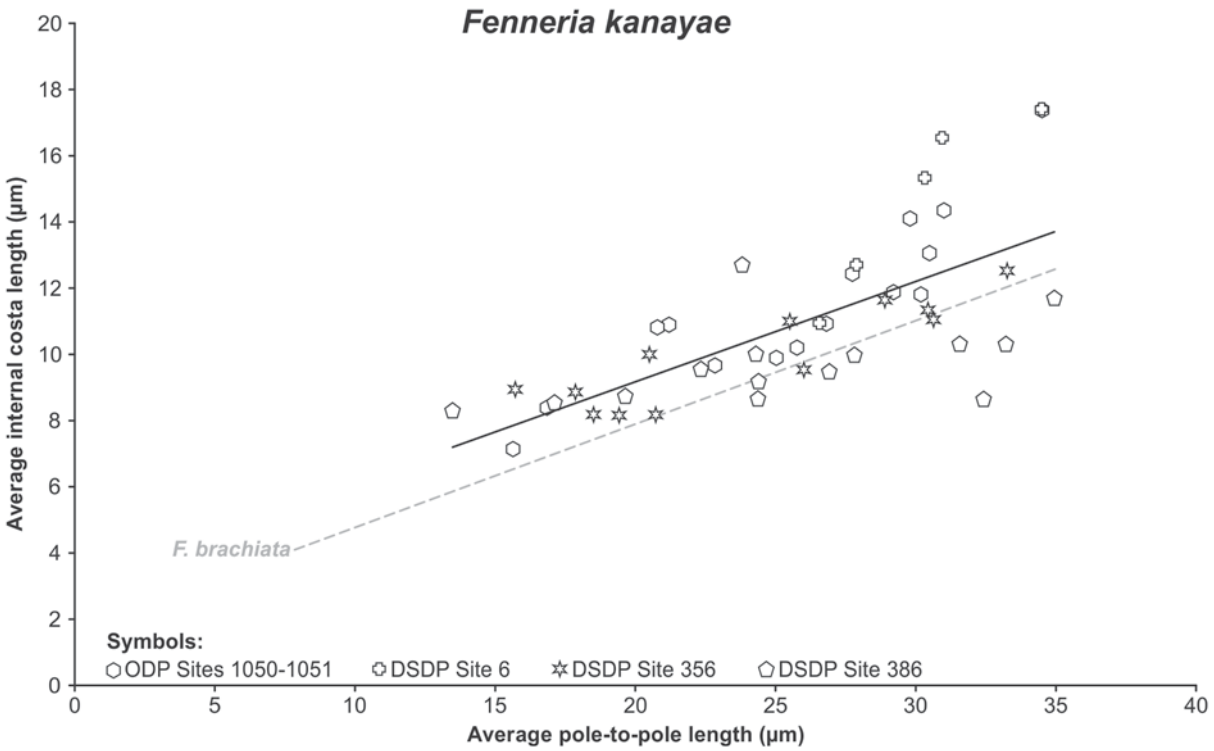

Text-fig. 6. Morphometry of *Fenneria kanayae* (Fenner) J. Witkowski, comb. nov. showing average pole-to-pole length plotted versus average internal costa length (see Box 1 in Text-fig. 3 for measurement explanation)

Hanna (1927) referred to this specimen as *Trinacria insipiens* Witt, 1886 (Witt 1886, p. 36, pl. 10, fig. 1; pl. 11, figs 5, 7, 11; pl. 12, fig. 2). Kanaya (1957), however, indicated that this identification was incorrect and referred this species as *Triceratium* sp. A.

Strelnikova (1974), in her study of well-preserved and diverse Campanian diatom assemblages from Western Siberia, synonymized *Triceratium* sp. A of Kanaya (1957) and *T. insipiens* Witt *sensu* Hanna (1927) with *Triceratium schulzii* Jousé, 1949 (Jousé 1949, p. 72, pl. 1, fig. 8). Despite the large difference in age between the Eocene Californian and Late Cretaceous Siberian deposits, Strelnikova (1974) based her conclusion on the presence of prominent internal costae in what she considered as *T. schulzii*.

The original description of *T. schulzii* (Jousé 1949, pp. 72, 73, pl. 1, fig. 8) was accompanied by a simple line drawing, showing a tripolar diatom with narrow, rounded, perforate poles that are distinctly cut off from the central area. Both the description and the type illustration show a series of short, parallel lines along each margin of the valve, interpreted by Jousé (1949) as costae. Neither the description nor the illustration, however, indicate the presence of any structure that could be interpreted as the internal radial costae within the distal parts of the projections. As parts of the Jousé sample suite were recently located (Witkowski *et al*. 2012b; McCartney *et al*. 2014), it was possible to verify whether *T. schulzii* and *T. kanayae* are conspecific. For this reason, Jousé's sample no. 21 (SZCZ 15270, see Appendix), with *T. schulzii* indicated on the accompanying catalogue card (Witkowski *et al*. 2012b), was examined herein.

Sample no. 21 contains valves of a small diatom that matches the description and illustration of *T. schulzii* (Text-fig. 7). It belongs to *Trinacria* Heiberg, 1863, because its poles are considerably raised over the central area (Text-fig. 7A). The purported costae illustrated by Jousé (1949, pl. 1, fig. 8), are likely shadows cast by the mantle, seen in many light micrographs of *Trinacria* spp. (e.g., Sims and Ross 1988, pl. 12, fig. 88). The valve interior reveals no transverse, circumferential nor radial costae present in *F. kanayae*. Also, pseudosepta are not observed in *T. schulzii sensu stricto*, and its mantle margin is smooth rather than serrated (Text-fig. 7B). As Jousé's (1949) paper was published long before the advent of SEM, and illustrated only with line drawings, *T. schulzii* remained poorly known. The only verified report of *T. schulzii* is from the Campanian–Maastrichtian in-

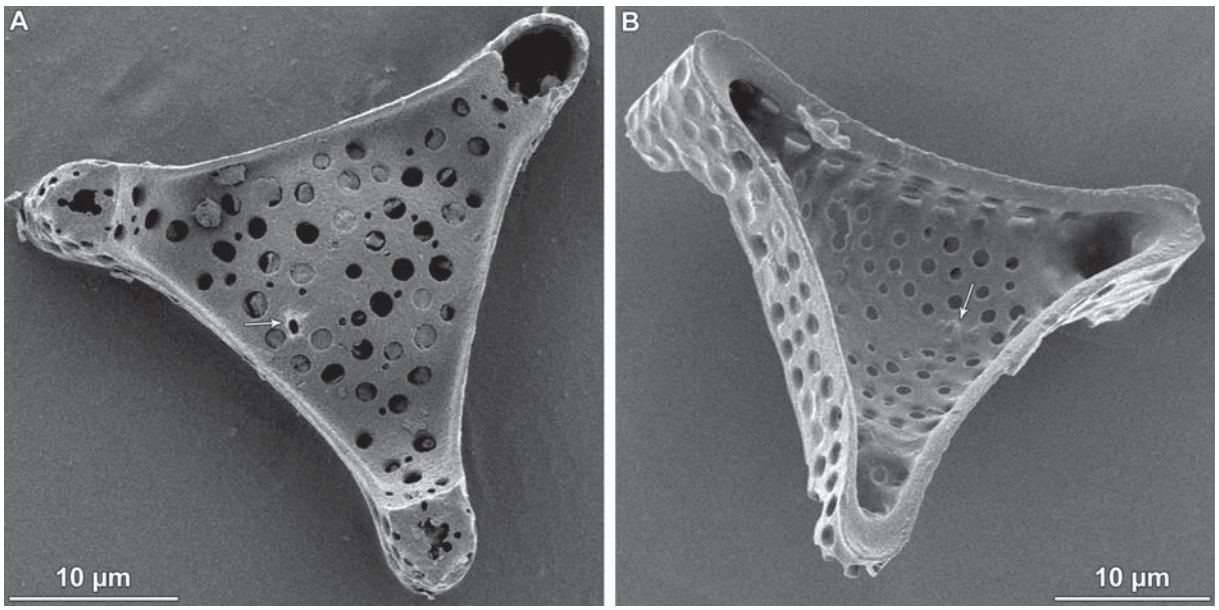

Text-fig. 7. Scanning electron micrographs showing valve morphology of *Triceratium schulzii* Jousé, 1949. A − External view; B − Oblique internal view. Arrows indicate the position of the rimoportula. Both specimens from sample SZCZ 15270, presumed type material from Jousé (1949; see the Appendix)

terval of DSDP Site 275 on the Campbell Plateau in the southwest Pacific Ocean (Hajós and Stradner 1975). Subsequent workers considered *T. schulzii sensu* Strelnikova (1974) as a synonym of *Medlinia deciusi* (Hanna) Nikolaev and Kociolek in Nikolaev *et al*., 2001 (Witkowski *et al*. 2011a). However, when Fenner (1977) used the name *T. schulzii* for an early Eocene diatom that she later named *T. kanayae*, there was considerable uncertainty concerning its stratigraphic range.

As in the case of *F. brachiata*, Gleser *et al*. (1986) transferred *T. kanayae* to *Lisitzinia*. The serrated mantle margin and considerably deeper mantle are the most important morphological characters to distinguish *F. kanayae* from *L. ornata* (Pl. 3, Figs 2, 3 versus Text-fig. 4). Moreover, *Fenneria* is a chain-forming genus, whereas no linking structures are observed on the valves of *L. ornata*. There is also a large temporal gap between the extinction of *F. kanayae* in the late early Eocene (see below) and the divergence of *Lisitzinia sensu stricto* in the late Oligocene (Scherer *et al*. 2007).

GEOGRAPHIC AND STRATIGRAPHIC DISTRIBUTION (Text-fig. 8; Table 3): *Fenneria kanayae* is reported from fewer localities than *F. brachiata*. However, *F. kanayae* occurs across a broad range of water depths, from coastal deposits (e.g., the Kellogg Shale) to pelagic sites (e.g., ODP Site 748). It has been reported from high southern to tropical and mid-northern latitude regions in the Indian and Atlantic oceans, respectively. In the Pacific Ocean, the only records of *F. kanayae* are from neritic sites in mid- and high northern latitudes (Text-fig. 8; Table 3).

Stratigraphically, reports of *F. kanayae* are more consistent than those of *F. brachiata* (Text-fig. 8). The southern high latitude records are temporally the youngest occurrences, which appear to coincide

Text-fig. 8. Stratigraphic and geographic distribution of *Fenneria kanayae* (Fenner) J. Witkowski, comb. nov. A − Stratigraphic distribution of → *F. kanayae* in datable deposits considered in this study plotted versus latitude. For essential stratigraphic information on the deposits included in this compilation see the Appendix and Table 3. Blue – Atlantic sites; green – Indian Ocean sites; red – Pacific sites; black – neritic and onshore sites. Dashed lines indicate approximate stratigraphic ranges. Solid lines indicate well-constrained stratigraphic ranges; B − Geographic distribution of *F. kanayae*. Site numbers correspond to numbers given to Text-figs 1 and 5, and Table 3 (column '#'). Base map plotted using Ocean Drilling Stratigraphic Network advanced plate tectonic reconstruction application (www.odsn.de). Numbers denote individual deposits, as listed in the lower right corner. Chronostratigraphy, magnetostratigraphy, and foraminiferal and nannofossil zonations follow Gradstein *et al.* (2012); radiolarian zonation follows Norris *et al.* (2014)

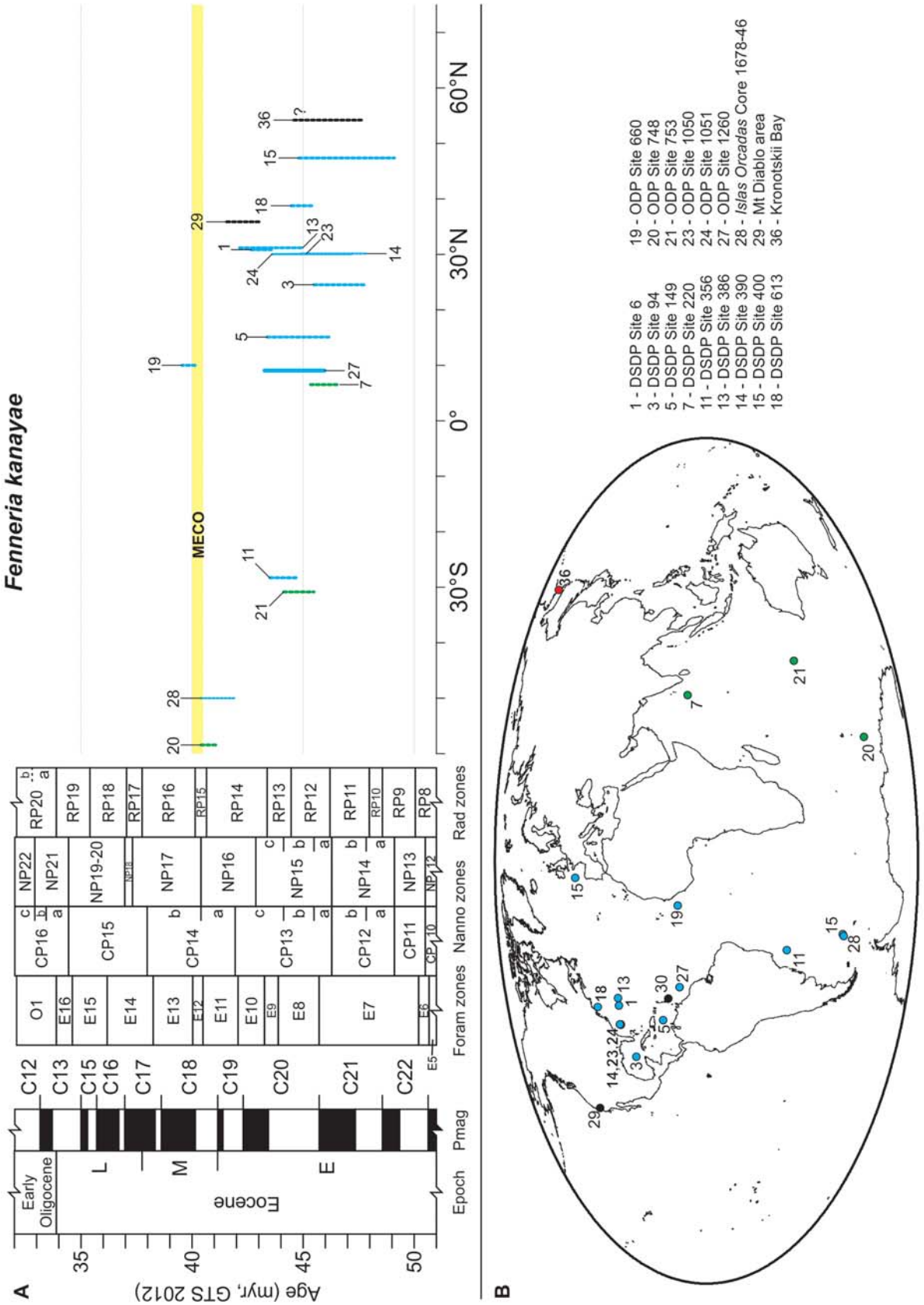
A
B
Fenneria kanayae
MECO
Age (myr, GTS 2012)
Epoch
Pmag
Foram zones
Nanno zones
Rad zones
Early Oligocene
Eocene
L
M
E
1 - DSDP Site 6
3 - DSDP Site 94
5 - DSDP Site 149
7 - DSDP Site 220
11 - DSDP Site 356
13 - DSDP Site 386
14 - DSDP Site 390
15 - DSDP Site 400
18 - DSDP Site 613
19 - ODP Site 660
20 - ODP Site 748
21 - ODP Site 753
23 - ODP Site 1050
24 - ODP Site 1051
27 - ODP Site 1260
28 - Islas Orcadas Core 1678-46
29 - Mt Diablo area
36 - Kronotskii Bay

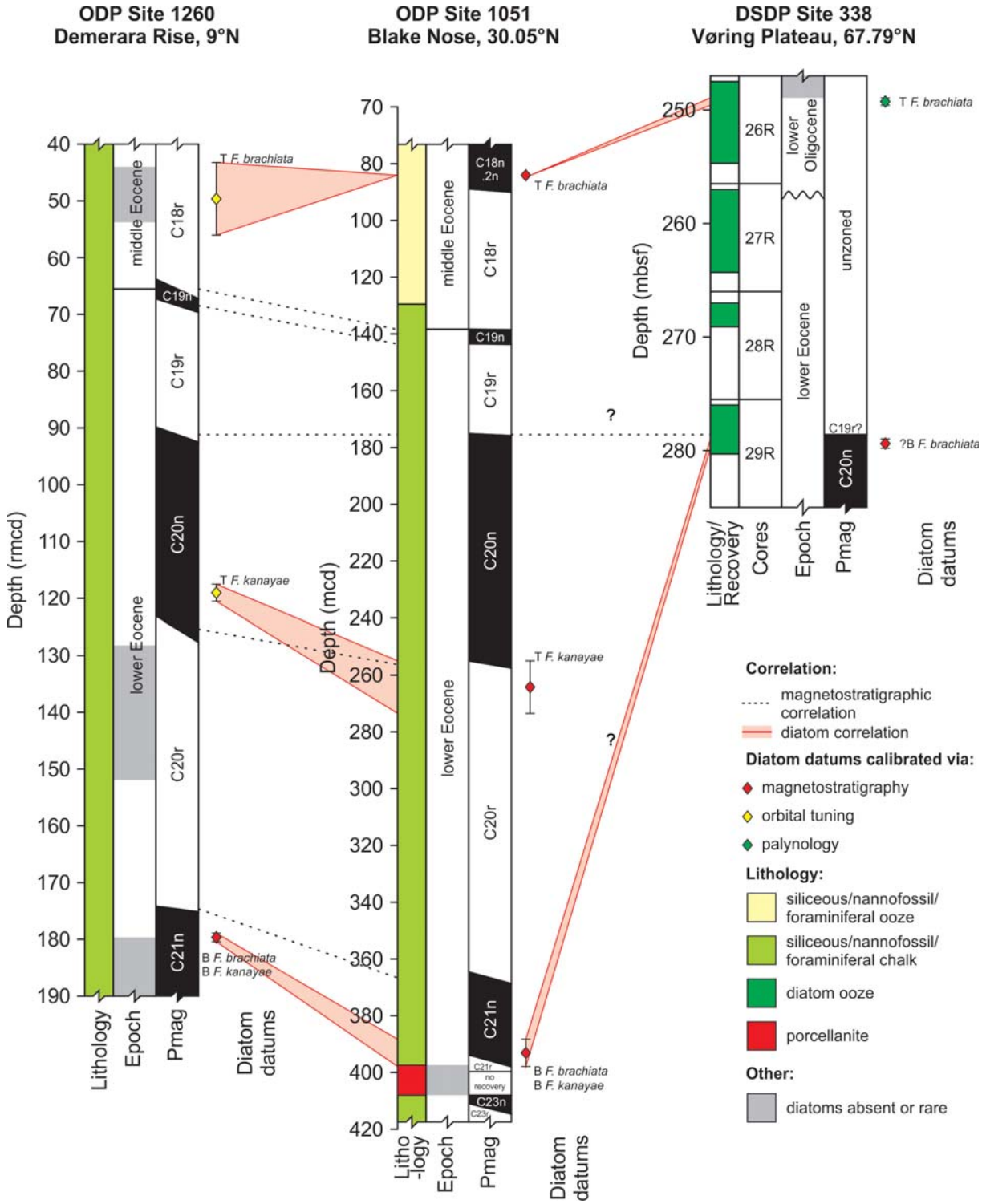

Text-fig. 9. Fence diagram showing the stratigraphic position of base (B) and top (T) for the stratigraphic ranges of *Fenneria kanayae* (Fenner) J. Witkowski, comb. nov. and *Fenneria brachiata* (Brightwell) J. Witkowski, comb. nov. at DSDP Site 338, and ODP Sites 1051 and 1260. Abbreviations: rmcd = revised metres composite depth; mcd = metres composite depth; mbsf = metres below sea floor; pmag = magnetostratigraphy. Site 1260 correlation based on data from: Erbacher *et al*. (2004), Suganuma and Ogg (2006), Renaudie *et al*. (2010), and Westerhold and Röhl (2013). Site 1051 correlation based on data from Norris *et al.* (1998b), Ogg and Bardot (2001), Edgar *et al.* (2010), and Luciani *et al.* (2016). Site 338 correlation based on data from Schrader and Fenner (1976), Dzinoridze *et al*. (1978, 1979) and Eldrett *et al.* (2004)

with the early phases of the MECO event (Text-fig. 8; Table 3). Only two mid-southern latitude records are available, but both fall within the late early Eocene.

The most numerous records of *F. kanayae* are from low- to mid-northern latitudes in the Atlantic Ocean (Text-fig. 8; Table 3). These records indicate a consistent stratigraphic range for *F. kanayae,* spanning the middle to late early Eocene. The only exception is Site 660 in the tropical Atlantic; Baldauf and Pokras (1989) reported *T. schulzii* from a single sample that likely falls within radiolarian zone RP16. This report likely represents reworking or misidentification.

Calibration of diatom datums

Most of the sites included in Table 3 and Text-figs 5 and 8 record only minor portions of the total stratigraphic ranges of *F. brachiata* and *F. kanayae*. The longest stratigraphic records are found at DSDP Site 338 in the Norwegian−Greenland Sea, ODP Site 1051 in the western North Atlantic, and ODP Site 1260 in the western tropical Atlantic. Reliable age control is available for all these sites. Thus, observations from Site 1051 presented here, supplemented by published data from Site 338 in the Norwegian−Greenland Sea (Schrader and Fenner 1976; Dzinoridze *et al.* 1978, 1979; Eldrett *et al*. 2004) and Site 1260 in the western tropical Atlantic (Suganuma and Ogg 2006; Renaudie *et al.* 2010; Westerhold and Röhl 2013) are used to calibrate the first and last occurrences of *F. brachiata* and *F. kanayae* (Text-fig. 9; Table 4).

At Site 1051 (Text-fig. 9; Table 4) both B *F. kanayae* and B *F. brachiata* are observed at 393.09±4.8 mcd, within lower magnetozone C21n, equivalent to ~47.19 Ma. T *F. kanayae* is placed at 264.22±9.27 mcd within upper chron C20r, dated at ~43.6 Ma. T *F. brachiata* has been shown by Witkowski *et al.* (2014) to coincide with the termination of the MECO peak warming phase at 84.07±0.15 mcd, within magnetozone C18n.2n (~40.04 Ma). This placement is followed in this study, albeit with a minor adjustment to the depth, here placed at a mid-point between the minimum and maximum depths for this datum (Text-fig. 9; Table 4).

A considerable difference is observed in the timing of the first occurrences between Sites 1051 and 1260. The data of Renaudie *et al.* (2010) from Site 1260 show B *F. brachiata* and B *F. kanayae* at 179.65±0.75 rmcd within upper magnetozone C21n, equivalent to ~45.96 Ma (Text-fig. 9; Table 4). This age is 1.23 million years (myr) younger than at Site 1051. The difference in timing of these diatom datums may be related to the latitudinal difference between Sites 1051 and 1260, but it may also be related to preservation, as B *F. brachiata* and B *F. kanayae* at Site 1260 occur immediately above the lowermost dissolution interval documented by Renaudie *et al.* (2010; Text-fig. 9; Table 4). Danelian *et al.* (2007), however, do not report either of these species from the interval of the nearby ODP Site 1259 extending below the base of the interval examined for diatoms by Renaudie *et al.* (2010). Therefore, preservational issues are not likely to significantly underestimate the age of B *F. kanayae* and B *F. brachiata* at Site 1260.

T *F. kanayae* at Site 1260 does not seem to be affected by preservation; using Renaudie's *et al.* (2010) range charts, this datum is interpreted here at 119.02±1.5 rmcd within lower magnetozone C20n (Text-fig. 9; Table 4). Using the orbital tuning tie points of Westerhold and Röhl (2013), the age of this level can be interpolated at 43.26 Ma, i.e., ~0.34 Ma younger than at Site 1051. Although this difference in timing may be influenced by latitudinal differences, the orbitally-tuned age model for Site 1260 should be considered superior to the magnetostratigraphic age model available for Site 1051. Should further improvements be made to the magnetostratigraphy of Site 1051 (see Edgar *et al*. 2010 and Luciani *et al.* 2016 for a discussion on the magnetostratigraphy of Ogg and Bardot 2001), the timing of T *F. kanayae* could potentially prove consistent between Sites 1051 and 1260.

T *F. brachiata* at Site 1260 is also ambiguous. Renaudie *et al*. (2010) record *F. brachiata* as rel-

Diatom event	ODP Site 1260 (9°N)			ODP Site 1051 (30.05°N)			DSDP Site 338 (67.79°N)		
	Depth (rmcd)	Chron	Age (Ma, GTS2012)	Depth (mcd)	Chron	Age (Ma, GTS2012)	Depth (mbsf)	Chron	Age (Ma, GTS2012)
T *F. brachiata*	49.645±6.395	C18r	40.38	84.07±0.15	C18n.2n	40.04	249.265±0.325	C12r? C13n?	<33.3
T *F. kanayae*	119.02±1.5	lower C20n	43.26	264.22±9.27	upper C20r	43.60	–	–	–
B *F. brachiata*	179.65±0.75	upper C21n	45.96	393.09±4.8	lower C21n	47.19	279.385±0.415	upper C20n?	–
B *F. kanayae*	179.65±0.75	upper C21n	45.96	393.09±4.8	lower C21n	47.19	–	–	–

Table 4. Calibration of diatom datums to the Geomagnetic Polarity Timescale (Gradstein *et al.* 2012). Abbreviations: B − base of taxon range; T − top of taxon range; rmcd − revised metres composite depth; mcd − metres composite depth; mbsf − metres below sea floor

atively abundant immediately below a barren interval spanning 53.79 through 44.00 rmcd (Text-fig. 9). Above this interval, *F. brachiata* is absent, despite high diatom abundance. If the upper and lower limits of the uppermost dissolution interval at Site 1260 are considered as the minimum and maximum depths for T *F. brachiata*, this datum is placed at 49.645±6.395 rmcd within chron C18r (Text-fig. 9). This level can be dated at 40.38 Ma using the orbital tuning tie points of Westerhold and Röhl (2013). This age is 0.34 myr earlier than T *F. brachiata* documented at Site 1051 by Witkowski *et al.* (2014) using the revised magnetostratigraphy of Edgar *et al.* (2010). Similar diachroneity in foraminiferal datums (Edgar *et al.* 2010) suggests that inconsistent timing of T *F. brachiata* may be related to latitudinal differences between ODP Sites 1260 and 1051. The implications of why the last occurrence of one of the most widespread early-to-middle Eocene diatoms coincides with the initial warming phase of the MECO in the equatorial sector of the Atlantic Ocean rather than the termination of the peak warming phase, as in the mid-latitude region, have yet to be fully explored.

B *F. brachiata* at DSDP Site 338 occurs at 279.385±0.415 mbsf (Schrader and Fenner 1976), within magnetozone C20n (Eldrett *et al.* 2004; Text-fig. 9; Table 4). This level is immediately above the base of the diatom-bearing interval, and thus the lower range of this species at Site 338 could potentially be truncated. The most striking difference in timing between the Norwegian Sea and lower latitude sites, however, concerns T *F. brachiata* at Site 338, which is documented by Schrader and Fenner (1976) at 249.265±0.325 mbsf. This level is subjacent to a dissolution interval, and thus it is likely also truncated. However, based on dinocyst datums (Table 2), this level should be placed within the lower Oligocene magnetozone C13n or C12r (Eldrett *et al.* 2004; Egger *et al.* 2016). Despite a major hiatus spanning the entire middle and upper Eocene at Site 338, it is highly unlikely that *F. brachiata* is reworked in the Oligocene, as it occurs continuously (Schrader and Fenner 1976; Dzinoridze *et al.* 1978). Egger *et al.* (2016) provide a GTS2012 calibration for the dinocyst datums T *Areosphaeridium diktyoplokum* and B *Chiropteridium galea*, with average ages of 33.4 and 33.3 Ma, respectively. As no additional tie points are available from Hole 338, these dates constrain a maximum age for T *F. brachiata* in the Norwegian–Greenland Sea basin, which is >6.64 myr younger than at Site 1051 and >6.98 myr younger than at Site 1260 (Text-fig. 9; Table 4).

DISCUSSION

Relationships of *Fenneria*

As advocated by Gleser (1975, 1986), and echoed by numerous other workers (e.g., Sims and Hendey 2002; Witkowski *et al.* 2015), *Triceratium sensu lato* represents a heterogenous collection of taxa that are not related closely enough to belong within one genus. This can be readily recognized by the lack of polar ocelli in most taxa placed in *Triceratium sensu lato.* In this respect, *Fenneria* represents another step in the ongoing revision of *Triceratium sensu lato.*

Valves of *Fenneria* are poroid, and it would seem that the Biddulphiaceae is the appropriate family to accommodate this genus. One of the distinguishing characters of biddulphioid diatoms has been the presence of polar pseudocelli (Ross and Sims 1971); however, as recently suggested by molecular data (Ashworth *et al.* 2013), the presence of pseudocelli does not define a monophyletic group. Until a more comprehensive understanding of the Biddulphiaceae is developed, *Fenneria* is provisionally placed in that family.

Both *F. brachiata* and *F. kanayae* are reported consistently to make an isochronous first occurrence (Fenner 1984a, 1985; Scherer *et al.* 2007; Renaudie *et al.* 2010; Barron *et al.* 2015). This observation is corroborated here. Coupled with the remarkably high morphological similarity, especially between smaller valves of both taxa (Text-fig. 6), this implies shared ancestry. It is proposed that *F. brachiata* and *F. kanayae* represent sister taxa. The identification which of the multipolar Palaeogene diatom genera could be the closest relative of *Fenneria*, however, presents more of a challenge.

The valve morphology of *Fenneria* is similar to some species currently placed in *Medlinia* Sims, 1998, especially *M. abyssorum* (Grunow) Sims, 1998, *M. fenestrata* (Witt) Sims, 1998, *M. simbirskiana* (Witt) Sims, 1998, and *M. deciusi* (Hanna) Nikolaev and Kociolek in Nikolaev *et al.*, 2001. These species have generally flat valves, often with cameo/intaglio linking structures located at the valve centre and on the polar projections, and internal costae. These morphological features are not observed in other species of *Medlinia*, including the generitype, *M. pseudoweissei* Sims, 1998, but also *M. weissei* (Grunow) Sims, 1998, *M. synica* (Strelnikova) Sims, 1998 and *M. uralensis* (Strelnikova) Sims, 1998. The rimoportulae in this group have prominent external tubes (Sims 1998), and the valve face undulations are more pronounced, often with a dome-shaped central area

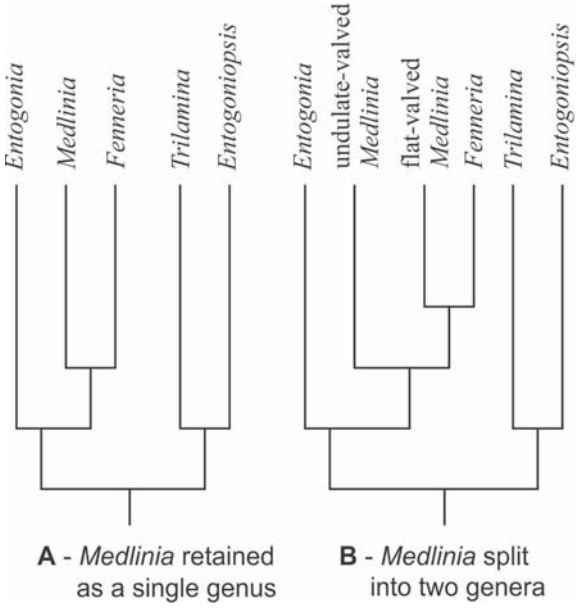

Text-fig. 10. Relationships among multipolar Palaeogene diatom genera as discussed in the text: *Entogonia* Greville, 1863, *Medlinia* Sims, 1998, *Fenneria* gen. nov., *Entogoniopsis* Sims, Strelnikova, Witkowski and Williams, 2015, and *Trilamina* Sims, Witkowski, Strelnikova and Williams, 2015, based on the relationships proposed by Witkowski *et al.* (2015, table 1 and fig. 253). A − with *Medlinia* retained as a single genus, despite morphological differences between flat-valved and undulate-valved taxa discussed in the text; B − with *Medlinia* split into two genera based on the presence or absence of valve face undulations

and transverse sulci across the polar projections. The sulci are perforated, in contrast to the hyaline internal costae of the flat-valved group (Sims 1998).

The primary reason why Sims (1998) grouped flat-valved and undulate taxa within *Medlinia* is the location of linking structures, both at the valve centre and at the poles, and the presence of prominent serrations along the mantle margin. These morphological characters could be interpreted as synapomorphies uniting the undulate- and flat-valved *Medlinia* spp. (Text-fig. 10A). Alternatively, the differences in valve face undulation patterns, length of the external tubes of the rimoportulae, and the presence or absence of sulci and internal costae, could suggest that *Medlinia* may require a division into two genera (Text-fig. 10B). However, further work on numerous taxa is needed to settle these issues.

Flat-valved *Medlinia* usually have transverse costae arranged in a similar pattern as in *F. brachiata*. No expansions of the free edge of internal costae comparable to *F. kanayae* have been documented for the flat-valved *Medlinia* spp. (Sims 1998), although some of these species have polar pseudosepta and complex networks of internal costae (see fig. 1f in Witkowski *et al.* 2011b for an internal view of *M. deciusi*). Even though the linking structures in *Fenneria* are not as pronounced as in the flat-valved *Medlinia*, it was certainly chain-forming (Pl. 4, Fig. 23; see also fig. 8.27 in Fenner 1985). Whenever present on valves of *Fenneria*, polar linking structures are also of the cameo/intaglio type (Pl. 3, Fig. 2; see also fig. 147 in Dzinoridze *et al.* 1979), either as grooves separated by ridges, or as rings of wedge-shaped bosses. Thus, the linking mechanism is another character common to *Fenneria* and flat-valved *Medlinia*, strongly suggesting a close phylogenetic relationship (Text-fig. 10).

It is beyond the scope of this study to resolve the taxonomic issues outlined above for *Medlinia*. Regardless, *Fenneria* should be considered as a genus closely related to *Medlinia sensu* Sims (1998; Text-fig. 10A), or, alternatively, to the group of flat-valved *Medlinia* species that differ morphologically from the generitype (Text-fig. 10B). Elaborating on the possible synapomorphies identified here, future studies may unite the latter group with *Fenneria*. Until this is accomplished, the above discussion is summarized in a cladogram in Text-fig. 10, which builds on the relationships proposed by Witkowski *et al.* (2015, table 1 and fig. 253).

Toward refining Palaeogene diatom biostratigraphy

In order to verify the diatom datum calibrations performed here, the ages listed in Table 4 are compared to those published by Barron *et al.* (2015) in their recent review of global Eocene diatom biostratigraphy. The age of B *F. brachiata* and B *F. kanayae* as reported by Barron *et al.* (2015, based on data from Scherer *et al.* 2007) is older than that established here (48.4 Ma versus 47.19 Ma, respectively). Whereas Scherer *et al.* (2007) state that these age estimates are based on John Barron's unpublished data from DSDP Hole 390A, they do not specify a depth for either of these events. One reason for this discrepancy could be the presence of a major recovery gap at ODP Site 1051 (Text-fig. 9). However, both the maximum and minimum depths for B *F. brachiata* and B *F. kanayae* are placed above this interval, making it unlikely to influence the calibration.

In the dataset of Barron *et al.* (2015), T *F. kanayae* and T *F. brachiata* are also isochronous at 39 Ma. Both datums are referenced as coming from Scherer *et al.* (2007), who did not, unfortunately, reveal the

depth for these events. Tables 3, 4 and Text-fig. 8 of the present study indicate that T *F. kanayae* has a considerably older age. Barron *et al.* (2015) distinguish between *T. barbadense* and *T. inconspicuum* in their dataset, with last occurrences dated at 40.3 and 39.0 Ma, respectively. For both these taxa, Barron *et al.* (2015) and the Barron Diatom Catalog published as part of the Lazarus *et al.* (2014) study make it clear that the authors considered Steven Bohaty's unpublished observations from ODP Site 1218. The calibration for *T. barbadense* in Barron *et al.* (2015) is largely consistent with T *F. brachiata* established here for Site 1260 (40.38 Ma). Both calibrations by Barron *et al.* (2015), however, disagree with the age of T *F. brachiata* established here for Site 1051. Clearly, further work is needed to settle this issue; however, the availability of multiple age calibrations for individual datums should be viewed a major progress in Palaeogene diatom biostratigraphy, which until recently lacked any calibration to the GPTS.

The latitudinal section through the North Atlantic presented in Text-fig. 9 and Table 4 shows that of the four diatom bioevents considered here (B *F. kanayae*, B *F. brachiata*, T *F. kanayae*, T *F. brachiata*), as many as three show a variable degree of diachroneity that is likely related to latitudinal differences. The only potentially isochronous datum is T *F. kanayae*, recorded at Sites 1051 and 1260. The 0.34 myr difference in timing between these two sites could result from age model imperfections and sampling resolution. The three remaining datums, however, display diachroneity that is too high to be attributed to age model imperfections.

Implications for diatom palaeobiogeography

It has been expressed that early Palaeogene diatoms showed little palaeobiogeographic provincialism (e.g., Fenner 1985; Gladenkov 2014; Lazarus *et al.* 2014). Whereas these authors refer to the Eocene–Oligocene Transition as a period of marked increase in provincialism, and not specifically to the preceding time interval, no quantitative perspective on Palaeogene diatom palaeobioegography has been put forward to date.

The present study identifies points of marked palaeobiogeographic differences between the tropical, subtropical, and subpolar regions as early as the early–middle Eocene transition. This is further emphasized by a comparison of the taxonomic composition of diatom assemblages reported from Chron C20n (42.301 to 43.432 Ma), the only time interval correlative between all three of the sites considered here (Sites 338, 1051 and 1260; see Table 5). Of the thirty-one presumably planktic diatom taxa included in this preliminary compilation, fewer than 10% occur at all sites. An equal proportion, nearly 13%, occurs in Chron C20n at Sites 338 and 1051, at Sites

Planktic diatoms occurring within Chron C20n	ODP Site 1260 Latitude 9°N	ODP Site 1051 Latitude 30.05°N	DSDP Site 338 Latitude 67.79°N
Brightwellia hyperborea	rare	absent	absent
Cestodiscus pulchellus	rare	absent	absent
Coscinodiscus bulliens	rare	absent	absent
Coscinodiscus decrescens	rare	absent	absent
Craspedodiscus oblongus	rare	absent	absent
Distephanosira architecturalis	rare	abundant	rare to common
Entogoniopsis foveata	absent	rare	absent
Fenneria brachiata	common	abundant	abundant
Fenneria kanayae	few	absent	absent
Hemiaulus alatus	few	absent	absent
Hemiaulus crenatus	absent	rare	absent
Hemiaulus gondolaformis	common	absent	absent
Hemiaulus grassus	abundant	absent	absent
Hemiaulus immanis	absent	rare	absent
Hemiaulus polycystinorum	abundant	rare	common
Medlinia abyssorum	absent	rare	absent
Odontella cornuta	absent	absent	common
Odontotropis carinata	absent	absent	rare
Odontotropis klavsenii	absent	absent	rare
Pyxilla gracilis	abundant	rare	absent
Quadrocistella spp	not counted	rare	absent
Riedelia claviger	absent	rare	rare
Riedelia pacifica	few	absent	absent
Rocella praenitida	absent	abundant	absent
Stephanopyxis corona	common	absent	absent
Stephanopyxis grunowii	few	absent	rare
Stephanopyxis mayenica	absent	absent	rare
Stephanopyxis barbadensis	absent	absent	rare to common
Stephanogonia pretiosa	absent	absent	rare to common
Triceratium acutangulum	absent	absent	rare
Trinacria quadrata	absent	absent	rare to common

Taxa present at all sites:	9.68%
Taxa present at sites 338 and 1051:	12.90%
Taxa present at sites 338 and 1260:	12.90%
Taxa present at sites 1051 and 1260:	12.90%

Table 5. Comparison of planktic diatom assemblage composition reported from DSDP Site 338, and ODP Sites 1051 and 1260. Data from: Schrader and Fenner (1976, Site 338), Renaudie *et al.* (2010, Site 1260), and Witkowski (unpublished) (Site 1051). Highlighted in grey are taxa that occur either at any pair of sites, or at all considered sites

1051 and 1260, and at Sites 338 and 1260 (Table 5). Most notably, however, the key zonal markers of the low latitude diatom zonation (Scherer *et al*. 2007; Barron *et al*. 2015; from bottom to top: *Hemiaulus incurvus*, *Pyxilla gracilis*, *Craspedodiscus oblongus*, *Pyxilla caputavis*, *Hemiaulus alatus*, *Hemiaulus gondolaformis*, *Brightwellia imperfecta*) are entirely absent or extremely rare at the mid-latitude Site 1051. On the other hand, *F. brachiata* is among the handful of taxa that occur in the tropical, subtropical and subpolar regions of the North Atlantic, albeit with considerable diachroneity (Text-fig. 9; Tables 3 and 5). Clearly, palaeobiogeographic diversification of diatoms took place considerably earlier than the Eocene−Oligocene Transition, and needs to be accounted for in biostratigraphic schemes. It is postulated here that a separate mid-latitude North Atlantic diatom biostratigraphic zonation could be developed to enhance temporal resolution and limit reliance on diachronous datums. Using the wealth of published palynological data (e.g., Eldrett *et al*. 2004; Egger *et al*. 2016) as a guide, such mid-latitude zonation is likely to enable a correlation between the diatom-bearing Norwegian-Greenland Sea sections and the existing robust low-latitude zonation (Fenner 1984a, 1985; Fourtanier 1991; Scherer *et al*. 2007; Barron *et al*. 2015). Ultimately, Palaeogene diatoms could become useful tools for correlation in the northern high-latitude diatom-bearing sites that initially had poor age control (e.g., DSDP Site 340, see Schrader and Fenner 1976; ODP Site 913, see Scherer and Koç 1996).

Fossil diatom field – where it is today and where it is heading

The fact that Palaeogene diatoms are largely understudied in comparison to other microfossil groups, and even in comparison to Neogene diatoms (e.g., Kemp *et al*. 1999; Crampton *et al*. 2016), is apparent but has received little formal discussion. This obviously hinders the potential application of early Cenozoic diatoms in modern Earth sciences.

Our understanding of the taxonomy, diversity, and geographic and stratigraphic distribution of fossil diatoms has made considerable progress since the seminal papers of Brightwell, Greville and other early workers. This progress has been achieved through two basic sources of information: (1) materials from onshore sites and (2) materials from ocean drilling.

Each of these have their advantages and disadvantages: the classic localities (e.g., Barbadian deposits; Kamyshlov, Kusnetzk, Ananino and other Russian sites) are often characterized by high diatom abundance and excellent preservation, but frequently represent samples of uncertain provenance, distributed among European diatomists in the 19th and early 20th centuries, under loosely applied names (Ross and Sims 1985; Oreshkina *et al*. 2004; Witkowski *et al*. 2015). Another complication is the lack of a stratigraphic context and age resolution. As some of these classical materials were not collected in a systematic geological manner, time series can be generated only in rare cases (see Witkowski *et al*. 2015 for discussion). Furthermore, the intense cleaning these samples had undergone also results in the elimination of smaller diatoms, leading to considerable taxonomic bias and a poorly constrained age. Finally, localities like the Barbados accretionary complex are characterized by an immensely complex geology, which further hinders stratigraphic correlation (e.g., Saunders *et al*. 1984; Harding and Lewis 1994). The extensive Palaeogene diatom-bearing sediments of central Russia and Kazakhstan are from thick stratigraphic successions, but often lack calcareous microfossils that would enable correlation to the deep-sea microfossil zonations (Oreshkina *et al*. 2004). Yet, intense work is being carried out in these sections (e.g., Oreshkina 2012; Oreshkina and Radionova 2014).

The deep-sea diatom-bearing deposits usually offer considerably better age control but a lower diatom abundance (e.g., Fenner 1984b; Witkowski *et al*. 2012a). They are often plagued by dissolution and/or other diagenetic processes acting against diatom preservation (e.g., zeolite or porcellanite/chert formation; Danelian *et al*. 2007 and Hesse 1988, respectively). Diatomists working with deep-sea Palaeogene materials often need to distinguish between allochthonous and *in situ* deposited valves (e.g., Witkowski *et al*. 2014). Finally, most deep-sea early Palaeogene diatom-bearing sections represent brief intervals of siliceous plankton production or discontinuous stratigraphic intervals (Barron *et al*. 2015), Site 1051 being a notable exception (Text-fig. 9).

What follows from this distinction is that Palaeogene taxonomic studies are often – but not exclusively (e.g., Harwood 1988; Sims and Ross 1990) – based on well-preserved shallow-water materials, whereas applied studies (i.e., biostratigraphically and palaeoceanographically-oriented) are usually based on deep-sea sections (e.g., Renaudie *et al*. 2010; but see also Barron *et al*. 1984). As a consequence, part of the extensive documentation of shallow-water Palaeogene taxa (e.g., Porguen and Sullivan 1997; Sims 2001, 2008; Sims and Hendey 2002), which has an immense importance for our understanding

of diatom evolution (e.g., as a means of testing phylogenetic hypotheses put forward based on molecular studies), has little relevance for interpreting palaeoenvironmental changes in the deep-sea record. Biostratigraphic and palaeoceanographic studies, on the other hand, often require a rapid pace, and thus tend to be based on LM examination only. The resultant biostratigraphic zonations, based on open-marine, often small-sized taxa such as *Fenneria*, are not readily applied to the observations based on heavily sieved residues from onshore sites kept in museum collections. Thus, the two realms tend to develop in isolation from one another.

In today's data mining age, this dichotomy has profound consequences for the entire Palaeogene diatom field. Deep-sea fossil diatom distribution data are incorporated into large online datasets (e.g., the Neptune or Pangaea databases). As numerous ocean drilling expeditions since the early ODP era had no diatomist on board, the quality of at least some of these data may be questionable. Yet, milestone work is often based on statistical treatment of Neptune (e.g., Lazarus *et al*. 2014) and other DSDP/ODP/IODP-related databases (e.g., Renaudie 2016). Presumably due to the lack of such syntheses for shallow-water environments, the conclusions from these works, although based nearly exclusively on the deep-sea realm, are assumed to relate to all diatoms living in a particular time period. High-profile palaeoceanographic studies, seeking insights on the possible role of diatoms in the Palaeogene ocean–atmosphere system, subsequently elaborate on such conclusions, leading to a highly speculative view of diatom ecological significance (e.g., Sexton *et al*. 2011; Ma *et al*. 2014). As a result, the extensive shallow-water diatom-bearing deposits that obviously point to high biosiliceous production in the early Palaeogene (Barron *et al*. 2015) are largely neglected in global palaeoceanographic reconstructions. Synthetic views of long time series will keep developing, and are likely to influence our views on diatom evolution to a still higher degree. Workers involved in fossil diatom studies need to ensure that data eventually incorporated into taxonomic or palaeoceanographic databases are of the highest quality.

It would appear from the above perspective that in order to bridge the utility gap between diatoms and other microfossil groups of the Palaeogene, first we need to bridge the gap within the diatom field itself. Linking data from the museum drawers and from ocean drilling in specimen-based studies (e.g., Sims and Ross 1990), including re-examination of extant type materials with a focus on morphometry, and geographic and stratigraphic distribution, can yield remarkable results in this respect. An especially informative example comes from the systematic study of fossil diatom resting spores, developed essentially from scratch over the last decade or so (e.g., Suto 2006a, b; Suto *et al*. 2008, 2009). Prior to the publication of these works, Palaeogene resting spore taxa were largely overlooked or lumped into few previously established genera, and had virtually no application in Earth sciences. Today, the importance of fossil diatom resting spores in reconstructing diatom evolution is acknowledged at a considerably higher degree (Harwood and Gersonde 1990), and *Chaetoceros* resting spores are successfully applied as palaeoproductivity proxies even in sediments of Cretaceous age (Davies *et al*. 2009). Thus, a refined taxonomic framework, so often disregarded, continues to be the basis for geologic utility of diatoms.

CONCLUSIONS

Using type materials from the Greville Collection at The Natural History Museum, London, UK, and observations from a range of onshore and deep-sea sites supplemented by a literature survey, two common early-to-middle Eocene diatoms, *Triceratium brachiatum* and *T. kanayae* are transferred to a new genus, *Fenneria*. The morphometry and nomenclatural history of *Triceratium inconspicuum* both indicate that this taxon is a synonym of *F. brachiata*. *Triceratium barbadense*, as revealed by Greville's original description and type slide, is a distinct species similar to *T. castellatum* West, and thus not part of the genus *Fenneria*.

Both B and T *F. brachiata* and B and T *F. kanayae* are calibrated to the GPTS based on published bio-, magneto- and cyclostratigraphic data from DSDP Site 338 and ODP Sites 1051 and 1260. These calibrations show a marked diachroneity in the diatom datums, likely due to palaeobiogeographic reasons.

A compilation of the geographic and stratigraphic distribution of *F. brachiata* and *F. kanayae* suggests pronounced palaeobiogeorgaphic provincialism in the early to middle Eocene oceans. This is against the widely held view that in the warmer climates of the early Palaeogene, diatom assemblages showed little palaeobiogeographic differentiation in distribution.

These preliminary observations have two important implications: (1) the tropical and northern high latitude Palaeogene diatom biostratigraphy is not fully applicable to the northern mid-latitudes and therefore a separate mid-latitude zonation should be

developed; and (2) with continued work on mid-latitude sections, and using the recent advances in other microfossil groups as a guide (e.g., Eldrett *et al*. 2004; Egger *et al*. 2016), considerable improvement can be achieved in Palaeogene northern high latitude biostratigraphy for the Atlantic Ocean. For these goals to be achieved, further specimen-based studies are required, combining the best available materials from museum collections and ocean drilling.

Acknowledgements

This work was supported by the Polish National Science Centre grant no. 2014/13/B/ST10/02988. Additional financial support for parts of this study was provided by the Foundation for Polish Science ("Start" programme), and by a European Commission Synthesys grant GB-TAF-1725, carried out within Framework Programme 7. Thanks are due to Patricia A. Sims, James Eldrett and David M. Harwood for insightful discussions. Andrew M. Gombos, Jr., and John A. Barron generously provided samples that were highly relevant to this study. Steven M. Bohaty is thanked for kindly sharing his unpublished data from Site 1218. Jean DeMouthe provided assistance in requesting samples from the California Academy of Sciences collections. David M. Williams provided advice on the contents of the Greville Herbarium. Yelena Polyakova and Maxim Kulikovskiy enabled a study of the Jousé sample suite. Andrey Gladenkov and Ekaterina Nikitina helped in obtaining relevant literature. Karolina Bryłka, Adrianna Szaruga, Julita Tomkowiak and Kevin McCartney helped with sample preparation. Additional thanks are due to Manfred Ruppel, Izabela Zgłobicka, Krzysztof Kurzydłowski, Łukasz Kruszewski and Anne Gleich. Finally, comments from two reviewers, David Harwood and David Williams, are greatly appreciated.

REFERENCES

Abbott, W.H. 1987. Diatom occurrences, Deep Sea Drilling Project sites 612 and 613. *Initial Reports of the Deep Sea Drilling Project*, **95**, 417–418.

Agnini, C., Fornaciari, E., Raffi, I., Catanzariti, R., Pälike, H., Backman, J. and Rio, D. 2014. Biozonation and biochronology of Paleogene calcareous nannofossils from low and middle latitudes. *Newsletters on Stratigraphy*, **47**, 131–181.

Andrews, J.E., Packham, G.H. and the Shipboard Scientific Party 1975. Site 289. *Initial Reports of the Deep Sea Drilling Project*, **30**, 231–398.

Anonymous, 1975. Proposals for a standardization of diatom terminology and diagnoses. *Nova Hedwigia*, *Beiheft*, **53**, 323–349.

Ashworth, M.P., Nakov, T. and Theriot, E.C. 2013. Revisiting Ross and Sims (1971): toward a molecular phylogeny of the Biddulphiaceae and Eupodiscaceae (Bacillariophyceae). *Journal of Phycology*, **49**, 1207–1222.

Baldauf, J.G. and Pokras, E.M. 1989. Diatom biostratigraphy of Leg 108 sediments: eastern tropical Atlantic Ocean. *Proceedings of the Ocean Drilling Program, Scientific Results*, **108**, 23–34.

Barron, J.A., Bukry, D. and Gersonde, R. 2014. Diatom and silicoflagellate biostratigraphy for the late Eocene: ODP 1090 (sub-Antarctic Atlantic). *Nova Hedwigia*, *Beiheft*, **143**, 1–32.

Barron, J.A., Bukry, D. and Poore, R.Z. 1984. Correlation of the middle Eocene Kellogg Shale of northern California. *Micropaleontology*, **30**, 138–170.

Barron, J.A., Stickley, C.E. and Bukry, D. 2015. Paleoceanographic, and paleoclimatic constraints on the global Eocene diatom and silicoflagellate record. *Palaeogeography*, *Palaeoclimatology*, *Palaeoecology*, **422**, 85–100.

Benson, W.E., Sheridan, R.E. and the Shipboard Scientific Party 1978. Sites 389 and 390: North Rim of Blake Nose. *Initial Reports of the Deep Sea Drilling Project*, **44**, 69–151.

Berggren, W.A., Kent, D.V., Swisher, III, C.C. and Aubry, M.P. 1995. A revised Cenozoic geochronology and chronostratigraphy. In: W.A. Berggren, D.V. Kent, M.-P. Aubry and J. Hardenbol (Eds.), *Geochronology, time scales and global stratigraphic correlation*. SEPM Special Publication, **54**, 129–212.

Berggren, W.A., Pessagno, Jr., G.A., Bukry, D. and Bramlette, M.N. 1969. Biostratigraphy. *Initial Reports of the Deep Sea Drilling Project*, **1**, 594–623.

Bohaty, S.M., Zachos, J.C., Florindo, F. and Delaney, M.L. 2009. Coupled greenhouse warming and deep-sea acidification in the middle Eocene. *Paleoceanography*, **24**, PA2207.

Brightwell, T. 1856. Further observations on the genus *Triceratium*, with descriptions and figures of new species. *Quarterly Journal of Microscopical Science*, **4**, 272–276.

Bukry, D. 1978. Cenozoic Silicoflagellate and Coccolith Stratigraphy, Northwestern Atlantic Ocean, Deep Sea Drilling Project, Leg 43. *Initial Reports of the Deep Sea Drilling Project*, **44**, 775–805.

Bukry, D. 1987. Eocene Siliceous and Calcareous Phytoplankton, Deep Sea Drilling Project Leg 95. *Initial Reports of the Deep Sea Drilling Project*, **95**, 395–415.

Cassidy, D. (Ed.) 1982. ARA *Islas Orcadas* Cruise 1678 Sediment Descriptions. *Sediment Research Laboratory Contribution*, **50**, 1–172.

Clarke, K.B. 1986. Thomas Brightwell's collection of diatom slides. *Transactions of the Norfolk & Norwich Naturalists' Society*, **27**, 178–182.

Crampton, J.S., Cody, R.D., Levy, R., Harwood, D., McKay, R. and Naish, T.R. 2016. Southern Ocean phytoplankton turn-

over in response to stepwise Antarctic cooling over the past 15 million years. *Proceedings of the National Academy of Sciences of the United States of America*, **113**, 6868−6873.

Danelian, T., Saint Martin, S. and Blanc-Valleron, M.-M. 2007. Middle Eocene radiolarian and diatom accumulation in the equatorial Atlantic (Demerara Rise, ODP Leg 207) – Possible links with climatic and palaeoceanographic changes. *Comptes Rendus Palevol*, **6**, 103−114.

Davies, A., Kemp, A.E.S. and Pike, J. 2009. Late Cretaceous seasonal ocean variability from the Arctic. *Nature*, **460**, 254−259.

Davies, A., Kemp, A.E.S., Weedon, G.P. and Barron, J.A. 2012. El Niño-Southern Oscillation variability from the Late Cretaceous Marca Shale of California. *Geology*, **40**, 15−18.

De Toni, G.B. 1894. Sylloge algarum omnium hucusque cognitarum. Vol. II. Bacillarieae. Sectio III. Cryptoraphideae, 1−956. Typis Seminarrii; Patavii.

Dinkelman, M.G. 1973. Radiolarian stratigraphy: Leg 16, Deep Sea Drilling Project. *Initial Reports of the Deep Sea Drilling Project*, **16**, 747−813.

Dzinoridze, R.N., Jousé, A.P., Koroleva-Golikova, G.S., Kozlova, G.E., Nagaeva, G.S., Petrushevskaya, M.G. and Strelnikova, N.I. 1978. Diatom and radiolarian Cenozoic stratigraphy, Norwegian Basin; DSDP Leg 38. *Initial Reports of the Deep Sea Drilling Project*, **38**−**41** (supplement), 289−428.

Dzinoridze, R.N., Jousé, A.P. and Strelnikova, N.I. 1979. Description of the diatoms. In: A.A. Strelkov and M.G. Petrushevskaya (Eds.), *The history of the microplankton of the Norwegian Sea*. Nauka, Moscow, 32−70.

Edgar, K.M., Wilson, P.A., Sexton, P.F., Gibbs, S.J., Roberts, A.P. and Norris, R.D. 2010. New biostratigraphic, magnetostratigraphic and isotopic insights into the Middle Eocene Climatic Optimum in low latitudes. *Palaeogeography*, *Palaeoclimatology*, *Palaeoecology*, **297**, 670−682.

Edgar, N.T., Saunders, J.B. and the Shipboard Scientific Party 1973. Site 146/149. *Initial Reports of the Deep Sea Drilling Project*, **15**, 17−168.

Egan, K.E., Rickaby, R.E.M., Hendry, K.R. and Halliday, A.N. 2013. Opening the gateways for diatoms primes Earth for Antarctic glaciation. *Earth and Planetary Science Letters*, **375**, 34−43.

Egger, L.M., Śliwińska, K.K., van Peer, T.E., Liebrand, D., Lippert, P.C., Friedrich, O., Wilson, P.A., Norris, R.D. and Pross, J. 2016. Magnetostratigraphically-calibrated dinoflagellate cyst bioevents for the uppermost Eocene to lowermost Miocene of the western North Atlantic (IODP Expedition 342, Paleogene Newfoundland sediment drifts). *Review of Palaeobotany and Palynology*, **234**, 159−185.

Ehrenberg, C.G. 1839. Über jetzt wirklich noch zahlreich lebende Thier-Arten der Kreideformation der Erde. *Bericht über die Bekanntmachung geeigneten Verhandlungen der Königlichen Preussischen Akademie der Wissenschaften zu Berlin*, **1839**, 152−159.

Ehrenberg, C.G. 1840. Über noch jetzt zahlreich lebende Thierarten der Kreidebildung und den Organismus der Polythalamien. *Abhandlungen der Königlichen Akademie der Wissenschaften zu Berlin*, **1839**, 81−174.

Eldrett, J., Harding, I.C., Firth, J.V. and Roberts, A.P. 2004. Magnetostratigraphic calibration of Eocene–Oligocene dinoflagellate cyst biostratigraphy from the Norwegian-Greenland Sea. *Marine Geology*, **204**, 91−127.

Erbacher, J., Mosher, D.C., Malone, M.J. and the Shipboard Scientific Party 2004. Site 1260. *Proceedings of the Ocean Drilling Program*, *Initial Reports*, **207**, 1−113.

Ewing, M., Worzell, J.L., Beall, A.O. and the Shipboard Scientific Party 1969. Site 6. *Initial Reports of the Deep Sea Drilling Project*, **1**, 243−292.

Exon, N.F., Kennett, J.P., Malone, M.J. and the Shipboard Scientific Party 2001. Site 1172. *Proceedings of the Ocean Drilling Program*, *Initial Reports*, **189**, 1−149.

Fenner, J. 1977. Cenozoic diatom biostratigraphy of the equatorial and southern Atlantic Ocean. *Initial Reports of the Deep Sea Drilling Project*, **39** (supplement), 491−624.

Fenner, J. 1984a. Eocene–Oligocene planktic diatom stratigraphy in the low latitudes and the high southern latitudes. *Micropaleontology*, **30**, 319−342.

Fenner, J. 1984b. Middle Eocene to Oligocene planktonic diatom stratigraphy from deep sea drilling sites in the South Atlantic, Equatorial Pacific, and Indian Oceans. *Initial Reports of the Deep Sea Drilling Project*, **75**, 1245−1271.

Fenner, J. 1985. Late Cretaceous to Oligocene planktic diatoms. In: H.M. Bolli, J.B. Saunders and K. Perch-Nielsen (Eds.), *Plankton Stratigraphy,* vol. 2, Cambridge University Press, 713−762.

Fourtanier, E. 1991. Paleocene and Eocene diatom biostratigraphy and taxonomy of eastern Indian Ocean Site 752. *Proceedings of the Ocean Drilling Program, Scientific Results*, **121**, 171−187.

Gladenkov, A.Yu. 2013. First finds of Eocene diatoms in the marine Paleogene reference section in the Il'pinskii Peninsula, northeastern Kamchatka. *Stratigraphy and Geological Correlation*, **21**, 96−106.

Gladenkov, A.Yu. 2014. Bipolar distribution of some earliest Oligocene marine diatoms. *Nova Hedwigia*, *Beiheft*, **143**, 337−368.

Gleser, S.I. 1969. Late Eocene complexes of diatoms, silicoflagellates and ebridians of the southwest part of Turgai Lowland. *Biostratigraficheskii Sbornik*, **4**, 67−85. [in Russian]

Gleser, S.I. 1975. To the revision of the genus *Triceratium* Ehr. sensu Hustedt, 1930 (Bacillariophyta). *Botanicheskii Zhurnal*, **60**, 1304−1313. [in Russian]

Gleser, S.I. 1986. On the position of the genus *Triceratium* s. str. (Bacillariophyta) in the diatom system. *Botanicheskii Zhurnal*, **71**, 1543−1545. [in Russian]

Gleser, S.I., Dolmatova, L.M. and Lupikina, E.G. 1986. Marine Paleogenic diatoms algae from eastern Kamchatka. *Botan-*

icheskii Zhurnal, **71**, 851−859. [in Russian with English abstract]

Gleser, S.I. and Jousé, A.P. 1974. Diatoms and silicoflagellates in the Eocene of the Equatorial Atlantic. In: A.P. Jousé (Ed.), *Mikropaleontologiya okeanov i morei*, Nauka, Moscow, 49−62 [in Russian with English summary]

Gleser, S.I., Jousé, A.P., Makarova, I.V., Proschkina-Lavrenko, A.I. and Sheshukova-Poretzkaya, V.S. (Eds.) 1974. *The diatoms of the USSR. Fossil and recent. Vol. I.* Nauka, Leningrad, 1−400. [in Russian]

Gleser, S.I., Zosimovitch, V.U. and Kljushnikov, M.N. 1965. Diatoms of Palaeogene deposits in the north Donetz basin and their stratigraphic position. *Paleontologicheskii Sbornik*, **2**, 73−90. [in Russian]

Gombos, A.M., Jr. 1982a. Early and middle Eocene diatom evolutionary events. *Bacillaria*, **5**, 225−242.

Gombos, A.M., Jr. 1982b. Three new and unusual genera of ebridians from the southwest Atlantic Ocean. *Journal of Paleontology,* **56**, 444−448.

Gombos, A.M., Jr. 1983. Middle Eocene Diatoms from the South Atlantic. *Initial Reports of the Deep Sea Drilling Project*, **71**, 565−581.

Gradstein, F.M., Ogg, J.G., Schmitz, M.D. and Ogg, G.M. 2012. The geologic time scale 2012. Elsevier, Amsterdam, 2 vols., 1−1144.

Greville, R.K. 1861a. Descriptions of new and rare diatoms. Series I. *Transactions of the Microscopical Society of London*, *New Series*, **9**, 39–45.

Greville, R.K. 1861b. Descriptions of new and rare diatoms. Series II. *Transactions of the Microscopical Society of London*, *New Series*, **9**, 67–73.

Greville, R.K. 1863. Descriptions of new and rare Diatoms. Series X. *Quarterly Journal of Microscopical Science*, *2nd series*, **3**, 227−237.

Hajós, M. and Stradner, H. 1975. Late Cretaceous Archaeomonadaceae, Diatomaceae, and Silicoflagellata from the South Pacific Ocean, Deep Sea Drilling Project, Leg 29, Site 275. *Initial Reports of the Deep Sea Drilling Project*, **29**, 913−1009.

Hanna, G. D. 1927. The lowest known Tertiary diatoms in California. *Journal of Paleontology*, **1**, 103−127.

Harding, I.C. and Lewis, J. 1994. Siliceous dinoflagellate thecal fossils from the Eocene of Barbados. *Palaeontology*, **37**, 825−840.

Harwood, D.M. 1988. Upper Cretaceous and lower Paleocene diatom and silicoflagellate biostratigraphy of Seymour Island, eastern Antarctic Peninsula. *Geological Society of America Memoir*, **169**, 55−129.

Harwood, D.M. and Bohaty, S.M. 2000. Marine diatom assemblages from Eocene and younger erratics, McMurdo Sound, Antarctica. In: J.D. Stilwell and R.M. Feldmann (Eds.), Paleobiology and paleoenvironments of Eocene rocks, McMurdo Sound, East Antartica. *Antarctic Research Series*, **76**, 73−98.

Harwood, D.M. and Gersonde, R. 1990. Lower Cretaceous Diatoms from ODP Leg 113 Site 693 (Weddell Sea). Part 2: Resting Spores, Chrysophycean Cysts, an Endoskeletal Dinoflagellate, and Notes on the Origin of Diatoms. *Proceedings of the Ocean Drilling Program, Scientific Results*, **113**, 403−425.

Harwood, D.M. and Maruyama, T. 1992. Middle Eocene to Pleistocene diatom biostratigraphy of Southern Ocean sediments from the Kerguelen Plateau, Leg 120. *Proceedings of the Ocean Drilling Program, Scientific Results*, **120**, 683−733.

Heiberg, P.A.C. 1863. *Conspectus criticus Diatomacearum Danicarum*. Wilhelm Priors Forlag, Copenhagen, 1−135.

Hesse, R. 1988. Diagenesis #13. Origin of chert: diagenesis of biogenic siliceous sediments. *Geoscience Canada*, **15**, 171−192.

Hollister, C.D., Ewing, J.I. and the Shipboard Scientific Party 1972. Site 108 – Continental Slope. *Initial Reports of the Deep Sea Drilling Project*, **108**, 357−364.

Jousé, A.P. 1949. New upper Cretaceous diatoms and silicoflagellates from clayey sands from the Bolshoy Aktai River basin (eastern slopes of Northern Urals). *Notulae Systematicae e Sectione Cryptogamica Instituti Nomine V. L. Komarovii Academiae Scientiarum U.R.S.S.*, **6**, 65–78. [in Russian]

Jousé, A.P. 1978. A new fossil diatom genus Lisitzinia (Bacillariophyta). In: A.P. Jousé (Ed.), *Morskaya Mikropaleontologiya* (*diatomei, radiolyarii, silikoflyagellyati, foraminifer'i i izvestkov'ii nannoplankton*), Nauka, Moscow, 47−48. [in Russian]

Kanaya, T. 1957. Eocene diatom assemblages from the Kellogg and "Sidney" Shales, Mt. Diablo Area, California. *Science Reports of the Tohoku University, Second Series* (*Geology*), **28**, 27−124.

Kemp, A.E.S., Pearce, R.B., Koizumi, I., Pike, J. and Jae Rance, S. 1999. The role of mat-forming diatoms in the formation of Mediterranean sapropels. *Nature*, **398**, 51−61.

Kützing, F.T. 1844. Die kieselschaligen Bacillarien oder Diatomeen, 1−152. Fritsch; Nordhausen.

Lazarus, D.B., Barron, J.A., Renaudie, J., Diver, P. and Türke, A. 2014. Cenozoic Planktonic Marine Diatom Diversity and Correlation to Climate Change. *PLoS ONE*, **9**, e84857.

Luciani, V., Dickens, G.R., Backman, J., Fornaciari, E., Giusberti, L., Agnini, C. and D'Onoforio, R. 2016. Major perturbations in the global carbon cycle and photosymbiont-bearing planktic foraminifera during the early Eocene. *Climate of the Past*, **12**, 981−1007.

Ludwig, W.J., Krasheninnikov, V.A. and the Shipboard Scientific Party 1983. Site 512. *Initial Reports of the Deep Sea Drilling Project*, **71**, 111−144.

Lyle, M., Wilson, P.A., Janecek, T.R. and the Shipboard Scientific Party 2002. Site 1218. *Proceedings of the Ocean Drilling Program, Initial Reports*, **199**, 1−126.

Ma, Z., Gray, E., Thomas, E., Murphy, B., Zachos, J. and Paytan, A. 2014. Carbon sequestration during the Palaeocene–Eocene Thermal Maximum by an efficient biological pump. *Nature Geoscience*, **7**, 382−388.

Manchester, S.R., Herrera, F., Fourtanier, E., Barron, J. and Martinez, J.-N. 2012. Oligocene age of the classic Belén fruit and seed assemblage of north coastal Peru based on diatom biostratigraphy. *The Journal of Geology*, **120**, 467−476.

Maxwell, A.E. and the Shipboard Scientific Party 1970. Site 13. *Initial Reports of the Deep Sea Drilling Project*, **3**, 27−70.

McCartney, K., Witkowski, J. and Kulikovskiy, M. 2014. Early Campanian silicoflagellates from the Ural Federal District, Russia: a taxonomic and biostratigraphic reexamination of the A.P. Jousé sample suite. *Micropaleontology*, **60**, 543–556.

Montadert, L., Roberts, D.G. and the Shipboard Scientific Party 1979. Sites 399, 400, and Hole 440A. *Initial Reports of the Deep Sea Drilling Project*, **48**, 35−71.

Müller, C. 1979. Calcareous Nannofossils from the North Atlantic (Leg 48). *Initial Reports of the Deep Sea Drilling Project*, **48**, 589−639.

Myhre, A.M., Thiede, J., Firth, J.V. and the Shipboard Scientific Party 1995. Site 913. *Proceedings of the Ocean Drilling Program*, *Initial Reports*, **151**, 345−382.

Nikolaev, V.A., Kociolek, J.P., Fourtanier, E., Barron, J.A. and Harwood, D.M. 2001. Late Cretaceous diatoms (Bacillariophyceae) from the Marca Shale Member of the Moreno Formation, California. *Occasional Papers of the California Academy of Sciences*, **152**, 1−119.

Norris, R.D., Kroon, R., Klaus, A. and the Shipboard Scientific Party 1998a. Site 1050. *Proceedings of the Ocean Drilling Program, Initial Reports,* **171B**, 93−169.

Norris, R.D., Kroon, R., Klaus, A. and the Shipboard Scientific Party 1998b. Site 1051. *Proceedings of the Ocean Drilling Program, Initial Reports,* **171B**, 171−240.

Norris, R.D., Willson, P.A., Blum, P. and the Shipboard Scientific Party 2014. Methods. *Proceedings of the Integrated Ocean Drilling Program*, **342**, 1−78.

Ogg, J. and Bardot, L. 2001. Aptian through Eocene magnetostratigraphic correlation of the Blake Nose Transect (Leg 171B), Florida Continental Margin. *Proceedings of the Ocean Drilling Program*, *Scientific Results*, **171B**, 1−58.

Okada, H. and Thierstein, H.R. 1979. Calcareous nannoplankton – Leg 43, Deep Sea Drilling Project. *Initial Reports of the Deep Sea Drilling Project*, **43**, 507−573.

Olshtynskaya, A.P. 2002. Morphological and taxonomic characteristics of some Paleogene diatoms of Ukraine. *International Journal on Algae*, **4**, 118−126.

Oreshkina, T.V. 2012. Evidence of Late Paleocene–Early Eocene hyperthermal events in biosiliceous sediments of Western Siberia and adjacent areas. *Austrian Journal of Earth Sciences*, **105**, 145−153.

Oreshkina, T.V., Aleksandrova, G.N. and Kozlova, G.E. 2004. Early Eocene marine planktonic record of the East Urals margin (Sverdlovsk region): biostratigraphy and paleoenvironments. *Neues Jahrbuch für Geologie und Paläontologie – Abhandlungen*, **234**, 201−222.

Oreshkina, T.V. and Radionova, E.P. 2014. Diatom record of the Paleocene–Eocene Thermal Maximum in marine paleobasins of Central Russia, Transuralia and adjacent regions. *Nova Hedwigia, Beiheft*, **143**, 307−336.

Paier, C. 2011. *Diatomáceas do Paleógeno do Platô de São Paulo* (*DSDP Leg 39, Site 356*). Unpublished Master Thesis, Universidade Do Vale Do Rio Dos Sinos, São Leopoldo. 1−81.

Pälike, H., Moore, T., Backman, J., Raffi, I., Lanci, L., Parés, J.M. and Janecek, T. 2005. Integrated Stratigraphic Correlation and Improved Composite Depth Scales for ODP Sites 1218 and 1219. *Proceedings of the Ocean Drilling Program, Scientific Results*, **199**, 1−42.

Peirce, J., Wiessel, J. and the Shipboard Scientific Party 1989. Site 753. *Proceedings of the Ocean Drilling Program*, *Initial Reports,* **121**, 171−189.

Perch-Nielsen, K. 1977. Albian to Pleistocene Calcareous nannofossils from the western South Atlantic, DSDP Leg 39. *Initial Reports of the Deep Sea Drilling Project*, **39**, 699−823.

Perch-Nielsen, K., Supko, R. and the Shipboard Scientific Party 1977a. Site 356: São Paulo Plateau. *Initial Reports of the Deep Sea Drilling Project*, **39**, 141−230.

Perch-Nielsen, K., Supko, R. and the Shipboard Scientific Party 1977b. Site 357: Rio Grande Rise. *Initial Reports of the Deep Sea Drilling Project*, **39**, 231−327.

Poag, C.W., Watts, A.B. and the Shipboard Scientific Party 1987. Site 613. *Initial Reports of the Deep Sea Drilling Project*, **95**, 155−241.

Porguen, V. and Sullivan, M.J. 1997. *Australodiscus peruvianus*, gen. et sp. nov., a marine centric diatom from the Peruvian Eocene. *European Journal of Phycology*, **32**, 119−124.

Proschkina-Lavrenko, A.I. 1949 (Ed.) *Diatom analysis. Vol. 2. Descriptions of fossil and recent diatoms. Orders Centrales and Mediales*. Botanicheskii Institut im V.L. Komarova Akademii Nauk S.S.S.R, 1−238. Gosudarstvennoe Izdatel'stvo Geologicheskoi Literatury; Moskva-Leningrad. [in Russian]

Radionova, E.P. 1996. Comparable study of Eocene diatoms from the oceanic and platform sections (North Atlantic and Russian Platform). In: K.I. Kusnetsova and N.G. Muzylöv (Eds.), Fossil microorganisms as the base of the Phanerozoic stratigraphy, correlation and paleobiogeography. *Voprosy Mikropaleontologii*, **31**, 83−101. [in Russian, with English abstract]

Renaudie, J. 2016. Quantifying the Cenozoic marine diatom deposition history: links to the C and Si cycles. *Biogeosciences*, **13**, 6003–6014.

Renaudie, J., Danelian, T., Saint Martin, S., Le Callonec, L. and Tribovillard, N. 2010. Siliceous phytoplankton response to a Middle Eocene warming event recorded in the tropical Atlantic (Demerara Rise, ODP Site 1260A). *Palaeogeography*, *Palaeoclimatology*, *Palaeoecology*, **286**, 121−134.

Riedel, W.R. and Sanfilippo, A. 1973. Cenozoic Radiolaria from the Caribbean, Deep Sea Drilling Project, Leg 15. *Initial Reports of the Deep Sea Drilling Project*, **15**, 705−751.

Roberts, A.P., Bicknell, S.J., Byatt, J., Bohaty, S.M., Florindo, F. and Harwood, D.M. 2003. Magnetostratigraphic calibration of Southern Ocean diatom datums from the Eocene−Oligocene of Kerguelen Plateau (Ocean Drilling Program sites 744 and 748). *Palaeogeography*, *Palaeoclimatology*, *Palaeoecology*, **198**, 145−168.

Ross, R., Cox, E.J., Karayeva, N.I., Mann, D.G., Paddock, T.B.B., Simonsen, R. and Sims, P.A. 1979. An amended terminology for the siliceous components of the diatom cell. *Nova Hedwigia*, *Beiheft*, **64**, 513−533.

Ross, R. and Sims, P.A. 1971. Generic limits in the Biddulphiaceae as indicated in the Scanning Electron Microscope. In: V.H. Heywood (Ed.), *Scanning Electron Microscopy, Systematic and Evolutionary Applications*, 155–177. Academic Press; London.

Ross, R. and Sims, P.A. 1985. Some genera of the Biddulphiaceae (diatoms) with interlocking linking spines. *Bulletin of the British Museum* (*Natural History*) *Botany Series*, **13**, 277−381.

Ruddiman, W., Sarnthein, M. Baldauf, J. and the Shipboard Scientific Party 1988. Site 660. *Proceedings of the Ocean Drilling Program*, *Initial Reports*, **108**, 327−407.

Saunders, J.B., Bernoulli, D., Müller-Merz, E., Oberhänsli, H., Perch-Nielsen, K., Riedel, W.R., Sanfilippo, A. and Torrini, R., Jr. 1984. Stratigraphy of the late Middle Eocene to Early Oligocene in the Bath Cliff section, Barbados, West Indies. *Micropaleontology*, **30**, 390−425.

Scherer, R.P. and Koç, N. 1996. Late Paleogene Diatom Biostratigraphy and Paleoenvironments of the Northern Norwegian−Greenland Sea. *Proceedings of the Ocean Drilling Program*, *Scientific Results*, **151**, 75−99.

Scherer, R.P., Gladenkov, A.Yu. and Barron, J.A. 2007. Methods and applications of Cenozoic marine diatom biostratigraphy. In: S.W. Starratt (Ed.), Pond scum to carbon sink: geological and environmental applications of the diatoms. *Paleontological Society Papers*, **13**, 61−83.

Schlich, R., Wise, Jr., S.W. and the Shipboard Scientific Party 1989. Site 748. *Proceedings of the Ocean Drilling Program*, *Initial Reports*, **120**, 157−235.

Schmidt, A. 1876. Atlas der Diatomaceen-Kunde, **20**, Plates 77−80. Ernst Schlegel's Verlag; Ascherleben.

Schmidt, R.R. 1978. Calcareous nannoplankton from the western North Atlantic DSDP Leg 44. *Initial Reports of the Deep Sea Drilling Project*, **44**, 703−729.

Schrader, H.-J. and Fenner, J. 1976. Norwegian Sea Cenozoic Diatom Biostratigraphy and Taxonomy. *Initial Reports of the Deep Sea Drilling Project*, **38**, 921−1099.

Sexton, P.F., Norris, R.D., Wilson, P.A., Pälike, H., Westerhold, T., Röhl, U., Bolton, C.T. and Gibbs, S. 2011. Eocene global warming events driven by ventilation of oceanic dissolved organic carbon. *Nature*, **471**, 349−353.

Shaw, C.A. and Ciesielski, P.F. 1983. Silicoflagellate Biostratigraphy of Middle Eocene to Holocene Sub-Antarctic Sediments Recovered by Deep Sea Drilling Project Leg 71. *Initial Reports of the Deep Sea Drilling Project*, **71**, 687−737.

Shibkova, K.G. 1968. Diatoms from the Palaeogene sediments of southern Kazakshtan. In: A.P. Jousé (Ed.), Iskopaem'ie diatomov'ye vodorosli SSSR, 21–26. Nauka; Moscow. [in Russian]

Sims, P.A. 1998. The early history of the Biddulphiales. I. The genus *Medlinia* gen. nov. *Diatom Research*, **13**, 337−374.

Sims, P.A. 2001. The genus *Praetriceratium* gen. nov.: a survey of eupodiscoid genera with a sipho marginalis. *Diatom Research*, **16**, 399−416.

Sims, P.A. 2008. *Ceratangula* gen. nov. is proposed together with a discussion on the genera *Cerataulus*, *Eupodiscus*, *Amphitetras*, *Amphipentas*, and *Diommatetras*. *Diatom Research*, **23**, 435−444.

Sims, P.A. and Hendey, N.I. 2002. A note on the valve structure of *Triceratium heterogonum* Barker & Meakin, an unusual species from Conset, Barbados. *Diatom Research*, **17**, 383−390.

Sims, P.A. and Ross, R. 1988. Some Cretaceous and Palaeogene *Trinacria* (diatom) species. *Bulletin of the British Museum* (*Natural History*). *Botany Series*, **18**, 275−322.

Sims, P.A. and Ross, R. 1990. *Triceratium pulvinar* and *T. unguiculatum*, two confused species. *Diatom Research*, **5**, 155−169.

Stickley, C.E., Brinkhuis, H., McGonigal, K.L., Chaproniere, G.C.H., Fuller, M., Kelly, D.C., Nürnberg, D., Pfuhl, H.A., Schellenberg, S.A., Schoenfeld, J., Suzuki, N., Touchard, Y., Wei, W., Williams, G.L., Lara, J. and Stant, S.A. 2004a. Late Cretaceous–Quaternary Biomagnetostratigraphy of ODP Sites 1168, 1170, 1171, and 1172, Tasmanian Gateway. *Proceedings of the Ocean Drilling Program, Scientific Results*, **189**, 1−57.

Stickley, C.E., Brinkuis, H., Schellenberg, S.A., Sluijs, A., Röhl, U., Fuller, M., Grauert, M., Huber, M., Warnaar, J. and Williams, G.L. 2004b. Timing and nature of the deepening of the Tasmanian Gateway. *Paleoceanography*, **19**, PA4027.

Strelnikova, N.I. 1974. Late Cretaceous diatoms, 1−201. Nauka; Moscow. [in Russian]

Strelnikova, N.I. 1992. Diatoms of the Palaeogene, 1−311. St. Petersburg University Press; St. Petersburg. [in Russian]

Suganuma, Y. and Ogg, J.G. 2006. Campanian through Eocene Magnetostratigraphy of Sites 1257–1261, ODP Leg 207,

Demerara Rise (Western Equatorial Atlantic). *Proceedings of the Ocean Drilling Program*, *Scientific Results*, **207**, 1–48.

Suto, I. 2006a. Taxonomy of the fossil marine diatom resting spore morpho-genera *Xanthioisthmus* Suto gen. nov. and *Quadrocistella* Suto gen. nov. in the North Pacific and Norwegian Sea. *Journal of Micropalaeontology*, **25**, 3–22.

Suto, I. 2006b. The explosive diversification of the diatom genus *Chaetoceros* across the Eocene/Oligocene and Oligocene/Miocene boundaries in the Norwegian Sea. *Marine Micropaleontology*, **58**, 259–269.

Suto, I., Jordan, R.W. and Watanabe, M. 2008. Taxonomy of the fossil marine diatom resting spore genus *Goniothecium* Ehrenberg and its allied species. *Diatom Research*, **23**, 445–469.

Suto, I., Jordan, R.W. and Watanabe, M. 2009. Taxonomy of middle Eocene diatom resting spores and their allied taxa from the central Arctic Basin. *Micropaleontology*, **55**, 259–312.

Talwani, M., Uditsev, G. and the Shipboard Scientific Party 1976. Sites 338–343. *Initial Reports of the Deep Sea Drilling Project*, **38**, 151–387.

Tsoy, I.B. 2003. Eocene diatoms and silicoflagellates from the Kronotskii Bay deposits (East Kamchatka). *Stratigraphy and Geological Correlation*, **11**, 71–86.

Tucholke, B.E., Vogt, P.R. and the Shipboard Scientific Party 1979. Site 386: fracture valley sedimentation on the central Bermuda Rise. *Initial Reports of the Deep Sea Drilling Project*, **43**, 195–321.

Valentine, P.C. 1987. Lower Eocene Calcareous Nannofossil Biostratigraphy Beneath the Atlantic Slope and Upper Rise off New Jersey – New Zonation Based on Deep Sea Drilling Project Sites 612 and 613. *Initial Reports of the Deep Sea Drilling Project*, **95**, 359–394.

van Andel, T.H. and Heath, G.R. 1973. Site 163. *Initial Reports of the Deep Sea Drilling Project*, **16**, 411–471.

Wade, B.S., Pearson, P.N., Berggren, W.A. and Pälike, H. 2011. Review and revision of Cenozoic tropical planktonic foraminiferal biostratigraphy and calibration to the geomagnetic polarity and astronomical time scale. *Earth-Science Reviews*, **104**, 111–142.

West, T. 1860. Remarks on some Diatomaceae, new or imperfectly described, and a new desmid. *Transactions of the Microscopical Society of London*, *New Series*, **8**, 147–153.

Westerhold, T. and Röhl, U. 2013. Orbital pacing of Eocene climate during the Middle Eocene Climate Optimum and the chron C19r event: missing link found in the tropical western Atlantic. *Geochemistry, Geophysics, Geosystems*, **14**, 4811–4825.

Whitmarsh, R.B., Weser, O.E., Ross, D.A. and the Shipboard Scientific Party 1974. Site 220. *Initial Reports of the Deep Sea Drilling Project*, **23**, 117–166.

Williams, D.M. 1988. An illustrated catalogue of the type specimens in the Greville diatom herbarium. *Bulletin of the British Museum* (*Natural History*) *Botany Series*, **18**, 1–148.

Wise, Jr., S.W. 1983. Mesozoic and Cenozoic Calcareous Nannofossils Recovered by Deep Sea Drilling Project Leg 71 in the Falkland Plateau Region, Southwest Atlantic Ocean. *Initial Reports of the Deep Sea Drilling Project*, **71**, 481–550.

Witkowski, J., Bohaty, S.M., Edgar, K.M. and Harwood, D.M. 2014. Rapid fluctuations in mid-latitude siliceous plankton production during the Middle Eocene Climatic Optimum (ODP Site 1051, western North Atlantic). *Marine Micropaleontology*, **106**, 110–129.

Witkowski, J., Bohaty, S.M., McCartney, K. and Harwood, D.M. 2012a. Enhanced siliceous plankton productivity in response to middle Eocene warming at Southern Ocean ODP Sites 748 and 749. *Palaeogeography*, *Palaeoclimatology*, *Palaeoecology*, **326–328**, 78–94.

Witkowski, J., Harwood, D.M. and Chin, K. 2011a. Taxonomic composition, paleoecology and biostratigraphy of Late Cretaceous diatoms from Devon Island, Nunavut, Canadian High Arctic. *Cretaceous Research*, **32**, 277–300.

Witkowski, J., Harwood, D.M. and Kulikovskiy, M. 2012b. Observations on Late Cretaceous marine diatom resting spore genera *Pseudoaulacodiscus* and *Archaegoniothecium* gen. nov. *Nova Hedwigia*, *Beiheft*, **141**, 375–404.

Witkowski, J., Sims, P.A. and Harwood, D.M. 2011b. Rutilariaceae redefined: a review of fossil bipolar diatom genera with centrally positioned linking structures, with implications for the origin of pennate diatoms. *European Journal of Phycology*, **46**, 378–398.

Witkowski, J., Sims, P.A., Strelnikova, N.I. and Williams, D.M. 2015. *Entogoniopsis* gen. nov. and *Trilamina* gen. nov. (Bacillariophyta): a survey of multipolar pseudocellate diatoms with internal costae, including comments on the genus *Sheshukovia* Gleser. *Phytotaxa*, **209**, 1–89.

Witt, O.N. 1886. Über den Polierschiefer von Archangelsk-Kurojedowo im Gouv. Simbirsk. *Verhandlungen der Russisch-kaiserlichen mineralogischen Gesellschaft zu St. Petersburg.* Series II, **22**, 137–177.

Worzel, J.L., Bryant, W. and the Shipboard Scientific Party 1973. Site 94. *Initial Reports of the Deep Sea Drilling Project*, **10**, 195–258.

Manuscript submitted: 12th June 2017
Revised version accepted: 7th December 2017

APPENDIX

Sources of specimens examined in this study

Specimens examined in SEM and LM:

(1) Deep Sea Drilling Project (DSDP) Leg 1, Site 6 (30.84º N, 67.65º W) was drilled in 5125 m of water on the Bermuda Rise (Text-fig. 1, locality #1), in the western North Atlantic Ocean (Ewing *et al*. 1969). Two late early Eocene samples from the A.L. Brigger Collection were examined in this study, curated at CAS under accession numbers 610596 and 610598 (Table A1). These samples are interpreted to belong to foraminiferal zones E9 to E10 (Berggren *et al*. 1969; Wade *et al*. 2011).

(2) DSDP Leg 71, Site 512 (49.87º S, 40.85º W) was drilled in 1846 m of water on the Maurice Ewing Bank (Text-fig. 1, locality #16), in the South Atlantic Ocean (Ludwig *et al*. 1983). Diatom and silicoflagellate biostratigraphy (Gombos 1983; Shaw and Ciesielski 1983) indicates a middle Eocene age, equivalent to calcareous nannofossil subzone CP14a (Wise 1983), for the siliceous nannofossil ooze recovered from Hole 512 between 20.2 and 89.3 mbsf. Gombos (1983) reported *T. inconspicuum* var. *trilobata* from this interval. Sample SZCZ 15067 was examined in this study (Table A1).

(3) Ocean Drilling Program (ODP) Leg 171B, Hole 1050B (30.10º N, 76.24º W). Site 1050 was drilled on Blake Nose in the Western North Atlantic Ocean (Text-fig. 1, locality #23). The siliceous nannofossil ooze and chalk recovered at Site 1050 spans the late early Palaeocene through middle Eocene (nannofossil zones NP5 to NP16; Norris *et al*. 1998a). One sample from MRC collections was examined in this study (Table A1).

(4) *Islas Orcadas* Cruise 1678, Core 46 (50.00º S, 42.18º W). Gombos (1982b) reported diverse assemblages of diatoms and ebridians from a series of piston cores taken aboard ARA *Islas Orcadas* from Maurice Ewing Bank in the South Atlantic Ocean (Text-fig. 1, locality #28). Core 1678-46 is composed of nannofossil ooze (Cassidy 1982), and foraminifer and diatom assemblages, including *T. barbadense*, indicate a middle Eocene age of this sediment, likely correlative with the *Globigeraspis index* foraminiferal zone (see also Ludwig *et al*. 1983). Andrew M. Gombos, Jr., generously shared part of his original sample set; sample SZCZ 18286 was examined in this study (Table A1).

(5) Kellogg Shale, California, USA (35.87º N, 121.67º W); Barron *et al*. (1984) published a comprehensive report on middle Eocene diatoms and silicoflagellates from the Kellogg Shale (Text-fig. 1, locality #29). According to Barron *et al*. (2015), this section correlates with the middle to upper part of nannofossil zone NP16. From the original sample suite generously shared by John Barron, sample CD-19 (outcrop elevation 18 m) showed the highest relative abundance of a diatom reported by Barron *et al*. (1984) as *T. inconspicuum*, and was therefore selected for examination in this study.

(6) Two additional samples were examined in SEM for comparative purposes only, and thus their stratigraphic context is not discussed in detail. SZCZ 15068 of late Oligocene age (Table A1) was used to examine the valve morphology of *L. ornata*. This sample comes from the flank of the Mid-Atlantic Ridge in the South Atlantic Ocean (Text-fig. 1, locality #17). SZCZ 15270 (sample no. 21 from the Jousé sample suite – see Witkowski *et al*. 2012b) is of Campanian age and comes from a locality labelled as Bolshoi Aktai River in Sverdlovsk District, Russia (Text-fig. 1, locality #32). It was used to examine the valve morphology of *T. schulzii*.

Specimens examined in LM only:

(1) DSDP Leg 38, Site 338 (67.79º N, 5.39º W) was drilled on the Vøring Plateau in the Norwegian–Greenland Sea (Text-fig. 1, locality #9), in 1297 m of water, and recovered remarkably rich diatom-bearing sediments of Miocene, Oligocene and Eocene age (Talwani *et al*. 1976). Schrader and Fenner (1976), and Dzinoridze *et al*. (1978) reported *T. barbadense* from the basal part of the diatom-bearing interval at this site. Despite the large abundance and excellent preservation of diatoms (Schrader and Fenner 1976; Dzinoridze *et al*. 1978, 1979), initial age control for the Palaeogene interval of Hole 338 was poor due to the scarcity of calcareous microfossils (Talwani *et al*. 1976). Dinocyst biostratigraphy (Eldrett *et al*. 2004) indicates a hiatus between the lower Eocene and lower Oligocene at ~257.5 mbsf. A robust magnetostratigraphy was also constructed for the bottom part of the hole. However, the diatom ooze interval between ~250 and 280 mbsf yielded a weak palaeomagnetic signal, which enabled only a tentative identification of the C19r/C20n reversal (Eldrett *et al*. 2004). Slide MRC D-005-220 was examined from Site 338 in this study (Table A1).

Repository	Sample no.	Leg	Site	Hole	Core	Type	Sc	Top (cm)	Bot (cm)	Sub-bottom depth
CAS	610596	1	6	–	3	–	3	87	93	192.3 mbsf
CAS	610598	1	6	–	4	–	1	57	63	229.8 mbsf
MRC	D-005-220	38	338	–	29	–	4	0	1	280 mbsf
MRC	D-005-230	39	356	–	6	R	3	50	51	117.5 mbsf
MRC	D-002-719	108	660	A	16	H	5	139	140	142.19 mbsf
MRC	D-002-720	108	660	A	17	X	2	54	55	146.04 mbsf
MRC	D-002-731	108	660	B	15	X	3	104	105	133.84 mbsf
MRC	D-002-732	108	660	B	15	X	5	39	40	136.19 mbsf
MRC	–	171B	1050	B	13	X	3	10	11	112.9 mbsf
SZCZ	15222	39	356	–	9	R	1	130	131	191.3 mbsf
SZCZ	**23882**	43	386	–	14	R	2	61	62	330.42 mbsf
SZCZ	**23885**	43	386	–	15	R	3	62	63	350.82 mbsf
SZCZ	**23886**	43	386	–	16	R	1	136	137	367.66 mbsf
SZCZ	**23888**	43	386	–	17	R	1	47	48	385.77 mbsf
SZCZ	15067	71	512	–	15	–	3	17	18	67.87 mbsf
SZCZ	15068	71	513	A	18	–	2	142	143	230.42 mbsf
SZCZ	15249	120	748	B	19	H	4	39	41	166.49 mbsf
SZCZ	14989	120	748	B	19	H	6	127	129	170.37 mbsf
SZCZ	17090	171B	1051	A	8	H	1	6	7	73.22 mcd
SZCZ	17100	171B	1051	A	9	H	1	66	67	83.32 mcd
SZCZ	17111	171B	1051	A	9	H	3	96	97	86.62 mcd
SZCZ	17113	171B	1051	A	9	H	4	6	7	87.22 mcd
SZCZ	17114	171B	1051	A	9	H	4	36	37	87.52 mcd
SZCZ	17115	171B	1051	A	9	H	4	66	67.5	87.82 mcd
SZCZ	17118	171B	1051	A	9	H	5	6	7	88.72 mcd
SZCZ	17121	171B	1051	A	9	H	5	96	97	89.62 mcd
SZCZ	17993	171B	1051	A	10	H	1	96	97	93.12 mcd
SZCZ	18006	171B	1051	A	10	H	4	36	37	97.02 mcd
SZCZ	17956	171B	1051	A	10	H	5	96	97	99.12 mcd
SZCZ	17957	171B	1051	A	10	H	5	126	127	99.43 mcd
SZCZ	18846	171B	1051	B	11	H	5	127	128	103.32 mcd
SZCZ	18851	171B	1051	B	12	H	6	96	97	113.87 mcd
SZCZ	18856	171B	1051	B	13	H	6	6	7	124.19 mcd
SZCZ	18859	171B	1051	B	14	H	6	6	7	134.79 mcd
SZCZ	18702	171B	1051	B	15	H	6	4	5	144.82 mcd
SZCZ	18708	171B	1051	B	16	X	6	6	7	154.47 mcd
SZCZ	18862	171B	1051	B	17	X	4	36	37	161.88 mcd
SZCZ	18282	171B	1051	A	19	X	4	126	127	184.44 mcd
SZCZ	21635	171B	1051	A	21	X	1	20	21	201.31 mcd
SZCZ	21636	171B	1051	A	22	X	2	25	26	212.71 mcd
SZCZ	21637	171B	1051	A	23	X	1	105	106	220.90 mcd
SZCZ	24552	171B	1051	A	23	X	3	85	86	223.7 mcd
SZCZ	24554	171B	1051	A	25	X	4	50	51	245.21 mcd
SZCZ	21638	171B	1051	A	26	X	3	100	101	254.95 mcd
SZCZ	21640	171B	1051	A	28	X	2	130	131	273.49 mcd
SZCZ	21641	171B	1051	A	29	X	3	50	51	284.85 mcd
SZCZ	21642	171B	1051	A	30	X	1	50	51	292.97 mcd
SZCZ	21643	171B	1051	A	31	X	1	50	51	300.92 mcd
SZCZ	21644	171B	1051	A	32	X	1	50	51	312.58 mcd
SZCZ	21645	171B	1051	A	33	X	1	50	51	322.23 mcd
SZCZ	24078	171B	1051	A	33	X	2	50	51	323.73 mcd
SZCZ	21646	171B	1051	A	34	X	1	50	51	331.73 mcd
SZCZ	24081	171B	1051	A	34	X	2	50	51	333.23 mcd
SZCZ	21647	171B	1051	A	35	X	1	50	51	341.47 mcd

Repository	Sample no.	Leg	Site	Hole	Core	Type	Sc	Top (cm)	Bot (cm)	Sub-bottom depth
SZCZ	21648	171B	1051	A	36	X	1	50	51	350.29 mcd
SZCZ	21649	171B	1051	A	37	X	1	50	51	359.29 mcd
SZCZ	21650	171B	1051	A	38	X	1	50	51	368.99 mcd
SZCZ	21651	171B	1051	A	39	X	1	50	51	378.69 mcd
SZCZ	21652	171B	1051	A	40	X	1	50	51	388.29 mcd
SZCZ	21653	171B	1051	A	41	X	1	50	51	397.89 mcd
SZCZ	21654	171B	1051	A	42	X	1	50	51	408.32 mcd
SZCZ	23789	171B	1051	A	42	X	2	50	51	409.82 mcd
SZCZ	23790	171B	1051	A	42	X	3	50	51	411.32 mcd
SZCZ	18286	1678	–	–	46	–	–	22	24	–

Table A1. List of deep-sea materials examined for this study, arranged by site and depth. Abbreviations: Sc – section; Bot – bottom; mbsf – metres below sea floor; mcd – metres composite depth. Repositories: CAS – California Academy of Sciences; MRC – IODP Micropaleontological Reference Center, University of Nebraska-Lincoln, USA; SZCZ – University of Szczecin, Poland

(2) DSDP Leg 39, Site 356 (28.29º S, 41.09º W) was drilled in 3175 m of water on the São Paulo Plateau (Text-fig. 1, locality #11), in the South Atlantic Ocean (Perch-Nielsen 1977). A nearly 200 m thick unit of lower Eocene sediments was recovered at Site 356, including a diatom-bearing siliceous ooze spanning calcareous nannofossil subzones NP15b−c (Fenner 1977; Perch-Nielsen *et al.* 1977a). Site 356 is the type locality of *T. kanayae*. Sample SZCZ 15222 and slide MRC D-005-230 were examined from Site 356 in this study (Table A1).

(3) DSDP Leg 43, Site 386 (31.19º N, 64.25º W) was drilled on the Bermuda Rise, western North Atlantic Ocean (Text-fig. 1, locality #13), in 4782 m of water. The Albian to Pleistocene succession recovered at Site 386 includes a ~350 m-thick interval of upper Palaeocene to middle Eocene turbidites, in part composed of biosiliceous sediments (Tucholke *et al.* 1979). To date, the only study of siliceous microfossils from Leg 43 cores is that of Bukry (1978), who documented well-preserved Palaeogene silicoflagellates in Hole 386. These were reported from a lower−middle Eocene radiolarian ooze interval between ~330 and ~385 mbsf. This unit spans calcareous nannofossil zones NP15b to NP16 (Okada and Thierstein 1979). Four samples from this interval (SZCZ 23882, 23885, 23886, 23888) were examined in this study (Table A1).

(4) ODP Leg 108, Site 660 (10.01º N, 19.25º W) was drilled in 4327.8 m of water within Kane Gap (Text-fig. 1, locality #19), adjacent to the Sierra Leone Rise in the eastern tropical Atlantic. A ~40 m thick interval of lower to middle Eocene radiolarian ooze correlative to radiolarian zones RP14 to RP16 was encountered in Holes 660A and 660B. Ruddiman *et al.* (1988), and Baldauf and Pokras (1989) reported *T. barbadense*, *T. brachiatum* and *T. inconspicuum*, as well as *T. schulzii* (= *T. kanayae*) from both holes. MRC slides D-002-719, D-002-720, D-002-731 and D-002-732 were examined from Site 660 (Table A1).

(5) ODP Leg 120, Hole 748B (58.43º S, 78.98º E) was drilled in 1290.9 m of water on the Southern Kerguelen Plateau (Text-fig. 1, locality #20), Southern Ocean (Schlich *et al.* 1989). Harwood and Maruyama (1992) were the first to examine the entire middle Eocene through Pleistocene diatom-bearing interval in this hole; they reported *T. inconspicuum* from the upper Eocene interval of Hole 748B; Witkowski *et al.* (2012a) reported *T. inconspicuum* var. *trilobata* and *T. kanayae* var. *kanayae* from calcareous nannofossil zone CP14a (early−middle Eocene transition). Samples SZCZ 14989 and 15284 from Witkowski *et al.* (2012a) were re-examined herein (Table A1).

(6) ODP Leg 171B, Site 1051 (30.05º N, 76.36º W) was drilled on Blake Nose in the Western North Atlantic Ocean (Text-fig. 1, locality #24), in 1983 m of water. The entire ~600 m thick sequence recovered at Site 1051 is composed of lower Palaeocene through middle Eocene (foraminiferal zones P1c to E12) siliceous nannofossil ooze and chalk, with subordinate porcellanite (Norris *et al.* 1998b). Witkowski *et al.* (2014) reported on moderately- to well-preserved diatom assemblages from a narrow interval spanning the Middle Eocene Climatic Optimum (MECO) event (Bohaty *et al.* 2009). The interval examined in this study extends from 417.4 to 73.2 mcd. This is equivalent to upper C23r to basal C18n.1r magnetozones (Ogg and Bardot 2001; Edgar *et al.* 2010; Luciani *et al.* 2016). Forty five samples from this interval (Table A1) were examined herein, including the slides from Witkowski *et al.* (2014).

(7) Barbados (Text-fig. 1, locality #30). For a recent discussion on the age of the numerous diatom-bearing deposits of Barbados the reader is re-

Slide no.	Collection	Locality on label	Comments	Reference
BM2079	Greville	Barbadoes deposit	Type slide for *T. barbadense*	Williams (1988)
BM2084	Greville	Barbadoes deposit	Type slide for *T. inconspicuum*	Williams (1988)
BM37698	Payne	Springfield, Barbadoes	Labelled as *T. brachiatum*	–
BM37699	Payne	Springfield, Barbadoes	Labelled as *T. brachiatum*	–
BM37876	Payne	Springfield, Barbadoes	Labelled as *T. inconspicuum*	–
BM37877	Payne	Springfield, Barbadoes	Labelled as *T. inconspicuum*	–
GC3280	Adams	Cambridge, Barbadoes	Labelled as *T. inconspicuum*	–
J5277	Adams	Springfield, Barbadoes	Labelled as *T. inconspicuum* and *T. brachiatum*	–

Table A2. List of the Natural History Museum (BM) slides examined in this study

ferred to Witkowski *et al*. (2015). Both Brightwell (1856) and Greville (1861a, b) reported their taxa only as coming from "Barbadoes earth", which may refer to any diatom-bearing sediment from Barbados ranging in age from the middle Eocene to the early Miocene. In order to determine whether or not *T. brachiatum*, *T. barbadense* and *T. inconspicuum* are conspecific, eight slides made of Barbadian materials were examined from the BM collections (Table A2).

Published records (data from the following fossil deposits are cited here based on a literature survey):

(1) DSDP Leg 3, Site 13 (6.04º N, 18.23º W) was drilled in 4585 m of water on the Sierra Leone Rise (Text-fig. 1, locality #2) in the eastern tropical Atlantic. Due to spot coring, the sedimentary succession is known only partially. An interval of early Eocene radiolarian ooze that is likely correlative with radiolarian zone RP13 was recovered in Holes 13 and 13A (Maxwell *et al*. 1970). It contains diverse and well-preserved diatom assemblages; *T. brachiatum* is among the diatoms reported by Gleser and Jousé (1974), and Fenner (1985).

(2) DSDP Leg 10, Site 94 (24.53º N, 88.47º W) was drilled in the Campeche Scarp region within the Gulf of Mexico (Text-fig. 1, locality #3), in 1793 m of water. Nearly 200 m of lower to upper Eocene foraminifer and/or nannofossil chalk with subordinate cherts was penetrated in Hole 94 (Worzel *et al*. 1973). Fenner (1984a) based part of her low-latitude Eocene-Oligocene tropical diatom zonation, which includes *T. kanayae* and *T. inconspicuum* as zonal markers, on the interval of Site 94 spanning the upper NP11 to lower NP15 nannofossil zones.

(3) DSDP Leg 11, Site 108 (38.77º N, 72.65º W) was drilled on the New Jersey continental slope, in the western North Atlantic (Text-fig. 1, locality #4), in 1815 m of water. Only two cores of early–middle Eocene siliceous chalk were recovered, likely correlative with foraminiferal zones E9 to E12 (Hollister *et al*. 1972; Wade *et al*. 2011). Fenner (1985, fig. 8.12) illustrated *T. inconspicuum* from Hole 108.

(4) DSDP Leg 15, Site 149 (15.10º N, 69.36º W) was drilled in the Venezuelan Basin of the Caribbean (Text-fig. 1, locality #5), in 3972 m of water (Edgar *et al*. 1973). Together with holes 94 and 390A, Hole 149 formed the basis of Fenner's (1984a) low-latitude Eocene diatom zonation. Fenner (1984a) examined the lower to middle Eocene calcareous radiolarian ooze and radiolarian nannofossil chalk interval between ~380 and ~280 mbsf that extends from the lower RP12 radiolarian zone to the RP15/RP16 transition (Riedel and Sanfilippo 1973).

(5) DSDP Leg 16, Site 163 (11.24º N, 150.29º W) was drilled in the eastern tropical Pacific Ocean in the vicinity of Clarion Fracture Zone (Text-fig. 1, locality #6), in 5230 m of water. A 70 m thick interval of lower to upper Eocene clayey radiolarian ooze spanning radiolarian zones RP11 to RP17 was penetrated at Site 163 (Dinkelman 1973; van Andel *et al*. 1973). Fenner (1984b) reported *T. inconspicuum* var. *trilobata* from this interval.

(6) DSDP Leg 23, Site 220 (6.52º N, 70.98º E) was drilled within the Arabian Basin of the Indian Ocean, north of the Maldives (Text-fig. 1, locality #7), in 4036 m of water. Approximately 150 m-thick lower and upper Eocene sediments overlie a basaltic basement at this site, including a 70 m thick unit of radiolarian- and spicule- rich nannofossil ooze and chalk that falls within radiolarian zone RP11 (Whitmarsh *et al*. 1974). Fenner (1984b) reported *T. inconspicuum* var. *trilobata* and *T. kanayae* from this interval.

(7) DSDP Leg 30, Site 289 (0.50º S, 158.51º E) was drilled on the northern Ontong Java Plateau in the tropical Pacific Ocean (Text-fig. 1, locality #8), at 2206 m of water depth. A ~55 m thick unit of middle to upper Eocene siliceous limestones spanning radiolarian zones RP15 through RP17 has been penetrated at Site 289 (Andrews *et al*. 1975). Fenner (1984b) reported *T. inconspicuum* var. *trilobata* from this interval.

(8) DSDP Leg 38, Site 340 (67.21º N, 6.31º W) was drilled in 1206 m of water on the Vøring Plateau (Text-fig. 1, locality #10) in the North Atlantic. Sediments recovered at Site 340 have undergone considerable halotectonic deformation (Talwani *et al.* 1976). Given the total absence of calcareous microfossils, the age control for this site is tentative. Schrader and Fenner (1976) reported *T. barbadense* from an interval of mixed middle and upper Eocene diatom ooze in Hole 340.

(9) DSDP Leg 39, Site 357 (35.56º S, 30.00º W) was drilled in 2086 m of water on the Rio Grande Rise (Text-fig. 1, locality #12). Although initially considered barren (Fenner 1977), Fenner (1984b) reported early Eocene diatoms, including *T. inconspicuum*, from a narrow interval of limestone (358.6 through 355.5 mbsf) correlative with nannofossil zone NP15 (Perch-Nielsen 1977; Perch-Nielsen *et al*. 1977b).

(10) DSDP Leg 44, Hole 390A (30.14º N, 76.11º W) was drilled on Blake Nose, Western North Atlantic (Text-fig. 1, locality #14), in 2665 m of water. The interval between 76 and 19 mbsf in Hole 390A is composed of lower Eocene siliceous nannofossil ooze spanning calcareous nannofossil zones NP12 to NP16 (Benson *et al.* 1978; Schmidt 1978). Gombos (1982a) and in part Fenner (1984a) based their diatom zonations on the examination of Hole 390A. Although she did not specify the core depth, Fenner (1984a) reported *T. kanayae* and *T. inconspicuum* var. *trilobata* from an interval of Hole 390A correlative with the mid-NP14 to mid-NP15 nannoplankton zones.

(11) DSDP Leg 48, Hole 400A (47.38º N, 9.2º W) was drilled on the Meriadzek Escarpment in the Bay of Biscay (Text-fig. 1, locality #15), in 4399 m of water (Montadert *et al.* 1979). The only diatom report from Leg 48 published to date is a biostratigraphic study by Radionova (1996), who reported *T. kanayae* and *T. brachiatum* from a siliceous claystone interval between 620 through 520 mbsf, correlative to the upper NP12 to lower NP16 calcareous nannofossil zones (Müller 1979).

(12) DSDP Leg 95, Site 613 (38.77º N, 72.51º W) was drilled on the New Jersey continental rise (Text-fig. 1, locality #18) in the western North Atlantic Ocean, at water depth of 2309 m. An expanded lower Eocene section was recovered between 577.5 and 278 mbsf, composed largely of siliceous to porcellanitic nannofossil chalk (Poag *et al*. 1987), spanning calcareous nannofossil zones CP9b to CP13b (Valentine 1987). Apart from Bukry (1987), who provided short notes on diatoms from Leg 95, and Abbott (1987), who tabulated diatom occurrences at Sites 612 and 613, including *T. schulzii* (presumably *T. kanayae*), no general report on diatoms from Leg 95 sites was published to date.

(13) ODP Leg 121, Site 753 (30.84º S, 93.6º E) was drilled on Broken Ridge (Text-fig. 1, locality #21), in the eastern Indian Ocean. To date, no diatom report was published from this site, but Peirce *et al*. (1989) indicate the presence of well-preserved diatoms – including *T. kanayae* and *T. inconspicuum* var. *trilobata* – within a lower Eocene nannofossil chalk unit correlative to calcareous nannofossil subzones CP13b to CP13c in Holes 753A and 753B.

(14) ODP Leg 151, Hole 913B (75.49º N, 6.95º E) was drilled in 3318.6 m of water in the East Greenland Basin (Text-fig. 1, locality #22) (Myhre *et al*. 1995). Scherer and Koç (1996) documented Palaeogene diatom assemblages, including *T. inconspicuum* var. *trilobata*, from a biosiliceous clay interval at this site. Initial age control for this interval was poor due to the lack of calcareous microfossils. By comparison to DSDP Site 338 (Schrader and Fenner 1976; Dzinoridze *et al*. 1978; Fenner 1985), Scherer and Koç (1996) assigned the diatom-bearing interval of Site 913 to two diatom zones: the *Actinoptychus irregularis* Zone of latest Eocene through earliest Oligocene age, and the *Trinacria excavata* forma *tetragona* Zone of middle Eocene age (Fenner 1985; Scherer and Koç 1996). Eldrett *et al*. (2004) constructed a robust dinocyst biomagnetostratigraphy for Hole 913B, which shows that the diatom-bearing interval between ~548 and ~466 mbsf spans magnetozones C18n to C16n in the middle to upper Eocene.

(15) ODP Leg 189, Site 1172 (43.96º S, 149.83º E) was drilled in 2621.9 m of water on the East Tasman Plateau (Text-fig. 1, locality #25), in the southwest Pacific Ocean. Eocene and Oligocene diatom-bearing sediments were recovered between 503.42 and 355.80 mbsf in Hole 1172A (Exon *et al*. 2001), correlative with magnetozones C21n to C11n (Stickley *et al.* 2004a). To date, no general report on diatoms has been published for Site 1172, but Stickley *et al.* (2004b) briefly mention *T. inconspicuum* in their palaeoceanographic reconstruction of the deepening of the Tasmanian Gateway, based on the findings from Site 1172.

(16) ODP Leg 199, Site 1218 (8.89º N, 135.37º W) was drilled in the central equatorial Pacific Ocean in 4828 m of water (Text-fig. 1, locality #26). A ~57 m thick unit of middle and upper Eocene nannofossil chalk and radiolarite overlies a basaltic basement at this site (Lyle *et al.* 2002). To date, no diatom report was published from Site 1218. Unpublished observations generously shared by Steven Bohaty, however, indicate the presence of *T. inconspicuum* in an inter-

val correlative with the upper CP14a to lower CP14b calcareous nannofossil zones (Pälike *et al*. 2005).

(17) ODP Leg 207, Site 1260 (9.05º N, 54.32º W). At Site 1260, two holes were drilled in 1899.7 m of water on the Demerara Rise (Text-fig. 1, locality #27), in the tropical western Atlantic (Erbacher *et al*. 2004). Renaudie *et al*. (2010) reported diverse and well-preserved early to middle Eocene diatoms from Hole 1260A, including *T. kanayae, T. brachiatum* and *T. inconspicuum*. Renaudie *et al*. (2010) also documented three intervals, in which diatoms are rare or absent, likely due to dissolution. In this study, diatom datums interpreted from Renaudie's *et al*. (2010) range charts are plotted on the revised composite depth scale of Westerhold and Röhl (2013). The interval between 190 and 40 rmcd spans magnetozones upper C21n to C18r, following the magnetostratigraphy of Suganuma and Ogg (2006). In addition, the upper part of the diatom-bearing interval at Site 1260 (above 135.62 rmcd) is astronomically tuned using the La2004 orbital solution (Westerhold and Röhl 2013).

(18) Mount Diablo area, California, USA (Text-fig. 1, locality #29). Kanaya (1957) reported *T. barbadense*, *T. inconspicuum* and *T. kanayae* from the Sidney and Kellogg shales, both units exposed in the area surrounding Mt. Diablo. In this paper, the stratigraphy of Barron *et al.* (1984) is applied also to the report of Kanaya (1957).

(19) Eastern Ukraine (Text-Fig 1, locality #31). Proschkina-Lavrenko (1949) listed *T. inconspicuum* as present in the Kharkov region and the Luhansk district of eastern Ukraine; however, she considered these localities as lower Oligocene. Gleser *et al*. (1965) reported *T. barbadense* and *T. inconspicuum* from Melovoye, Staroverovka, Brazhniki, Kharkov, Bolshaya Babka and Komsomolskoe localities, all within the Kharkov District in eastern Ukraine. Gleser *et al*. (1974) also listed *T. barbadense* as present in Ukrainian localities. Olshtynskaya (2002), following the taxonomic concepts of Gleser *et al*. (1986), reported *Lisitzinia inconspicua* from the upper Eocene beds of Nikol'skoe village in the Luhansk District, eastern Ukraine.

(20) Yekaterinburg (formerly Sverdlovsk) District, Russia (Text-fig. 1, locality #32). Proschkina-Lavrenko (1949) listed *T. brachiatum* as occurring in the upper Eocene beds of the Sverdlovsk District.

(21) Aktobe region, Kazakhstan (Text-fig. 1, locality #33). SP-1 Borehole, drilled 40 km to the northwest of Aktobe, Kazakhstan, penetrated nearly 200 m of Palaeogene sediments. Radionova (1996) reported *T. inconspicuum* and '*T. kanayae* var. *trilobata*' from the *Amphitetras producta* diatom zone, correlative with the mid-NP14 to upper NP15 nannofossil zones.

(22) Turgai Basin, Kazakhstan (Text-fig. 1, locality #34). Gleser (1969) reported '*T. barbadensis*' from the upper Eocene sediments in the vicinity of Irgiz, located within the Turgai river basin in Kazakhstan. Gleser *et al*. (1974) also listed *T. barbadense* from western Kazakhstan.

(23) Ayakkuduk region, Uzbekistan (Text-fig. 1, locality #35). Shibkova (1968) reported abundant *T. barbadense* in the upper Eocene sediments recovered from core no. 19, taken in the Ayakkuduk region, Uzbekistan.

(24) Kamchatka, Russia (Text-fig 1, localities #36 and #37). Gleser *et al*. (1986) and Tsoy (2003) reported Eocene diatoms from a number of sites located in Kamchatka, including the Ol'ga and Kronotskii canyons (Text-fig 1, locality #36). Taxa examined here have been documented in both these reports. Tsoy (2003) correlated the diatom assemblages with mid- to upper NP14 to NP19/20 calcareous nannofossil zones. Gladenkov (2013) reported on diatoms from the Il'pinskii Peninsula (Text-Fig 1, locality #37), in the north-eastern part of Kamchatka. *Triceratium inconspicuum* is reported from a concretion sample that is likely correlative with the upper P9 foraminiferal zone (Berggren *et al.* 1995; = E7 of Wade *et al.* 2011; Gladenkov 2013).

(25) McMurdo Sound, East Antarctica (Text-fig 1, locality #38). Harwood and Bohaty (2000) described diverse, moderately- to well-preserved assemblages of diatoms from glacial erratics dubbed the 'McMurdo Erratics'. *Triceratium inconspicuum* var. *trilobata* was reported from erratic MtD-95 collected on Mount Discovery, and dated at middle Eocene.

PLATES 1–4

PLATE 1

Scanning electron micrographs of *Fenneria brachiata* (Brightwell) J. Witkowski, comb. nov.

1 − Oblique girdle view of frustule. Note slightly raised poles, and spinules on central area (arrowhead); CD19, Kellogg Shale

2 − Detail of slightly raised pole showing lack of any kind of polar perforation fields; CD19, Kellogg Shale

3-5 − External views showing variation in valve outline with decreasing valve diameter; 3 – ODP 171B-1050B-13X-3, 10−11 cm (MRC), Blake Nose; 4-5 – CD19, Kellogg Shale

6-8 − Internal views showing variation in valve outline. Note internal openings of rimoportulae proximal to internal costae (arrows); 6 − DSDP 1-6-4-1, 57−63 cm (Brigger Collection, CAS 610598), Bermuda Rise; 7 − DSDP 71-512-15-3, 17−18 cm (SZCZ 15067), Falkland Plateau; 8 − *Islas Orcadas* Core 1678-48, 22−24 cm (SZCZ 18286), Falkland Plateau

9 − Detail of external opening to rimoportula (arrowhead); CD19, Kellogg Shale

10 − Detail of internal opening to rimoportula, piercing internal costa (arrowhead); CD19, Kellogg Shale

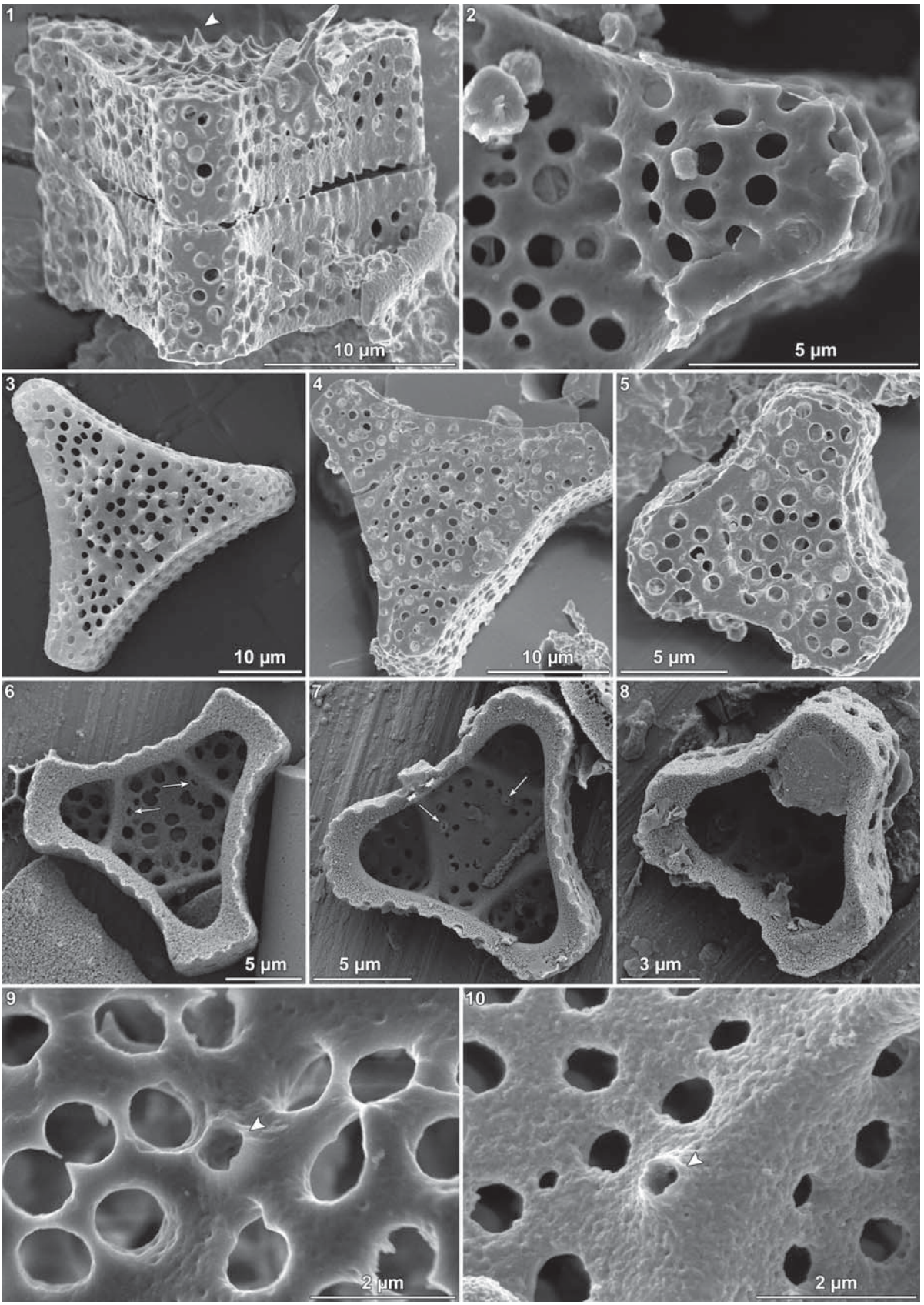
1
10 µm
2
5 µm
3
10 µm
4
10 µm
5
5 µm
6
5 µm
7
5 µm
8
3 µm
9
2 µm
10
2 µm

PLATE 2

Light micrographs of *Fenneria brachiata* (Brightwell) J. Witkowski, comb. nov.

1-30 − Valve views. 1 − BM 37699 (Springfield, Barbados); 2, 5, 8, 10, 13-14 − BM 37876 (Springfield, Barbados); 3, 15 – BM 37698 (Springfield, Barbados); 4, 7 – BM 2084 (Barbados); 4. is of the neotype; 6 − SZCZ 15249 (ODP 120-748B-19H-4, 39−41 cm, Kerguelen Plateau); 9 − BM Adams GC 3280 (Cambridge, Barbados); 11, 18 − BM 37877 (Springfield, Barbados); 12 – BM 37699 (Springfield, Barbados); 16-17 − SZCZ 17956 (ODP 171B-1051A-10H-5, 96−97 cm, Blake Nose); 19 − SZCZ 17957 (ODP 171B-1051A-10H-5, 126−127 cm, Blake Nose); 20 − SZCZ 17111 (ODP 171B-1051A-9H-3, 96−97 cm, Blake Nose); 21, 23 − SZCZ 17114 (ODP 171B-1051A-9H-4, 36−37 cm, Blake Nose); 22 − SZCZ 17118 (ODP 171B-1051A-9H-5, 6−7 cm, Blake Nose); 24 − SZCZ 14989 (ODP 120-748B-19H-6, 127−129 cm, Kerguelen Plateau); 25 − SZCZ 17115 (ODP 171B-1051A-9H-4, 66−67 cm, Blake Nose); 26 − SZCZ 17113 (ODP 171B-1051A-9H-4, 6−7 cm, Blake Nose); 27 − SZCZ 17121 (ODP 171B-1051A-9H-5, 96−97 cm, Blake Nose); 28 − SZCZ 17118 (ODP 171B-1051A-9H-5, 6−7 cm, Blake Nose); 29 − SZCZ 18006 (ODP 171B-1051A-10H-4, 36−37 cm, Blake Nose); 30 − SZCZ 15067 (DSDP 71-512-15-3, 17−18 cm, Falkland Plateau)

31 − Girdle view; BM 37876 (Springfield, Barbados)

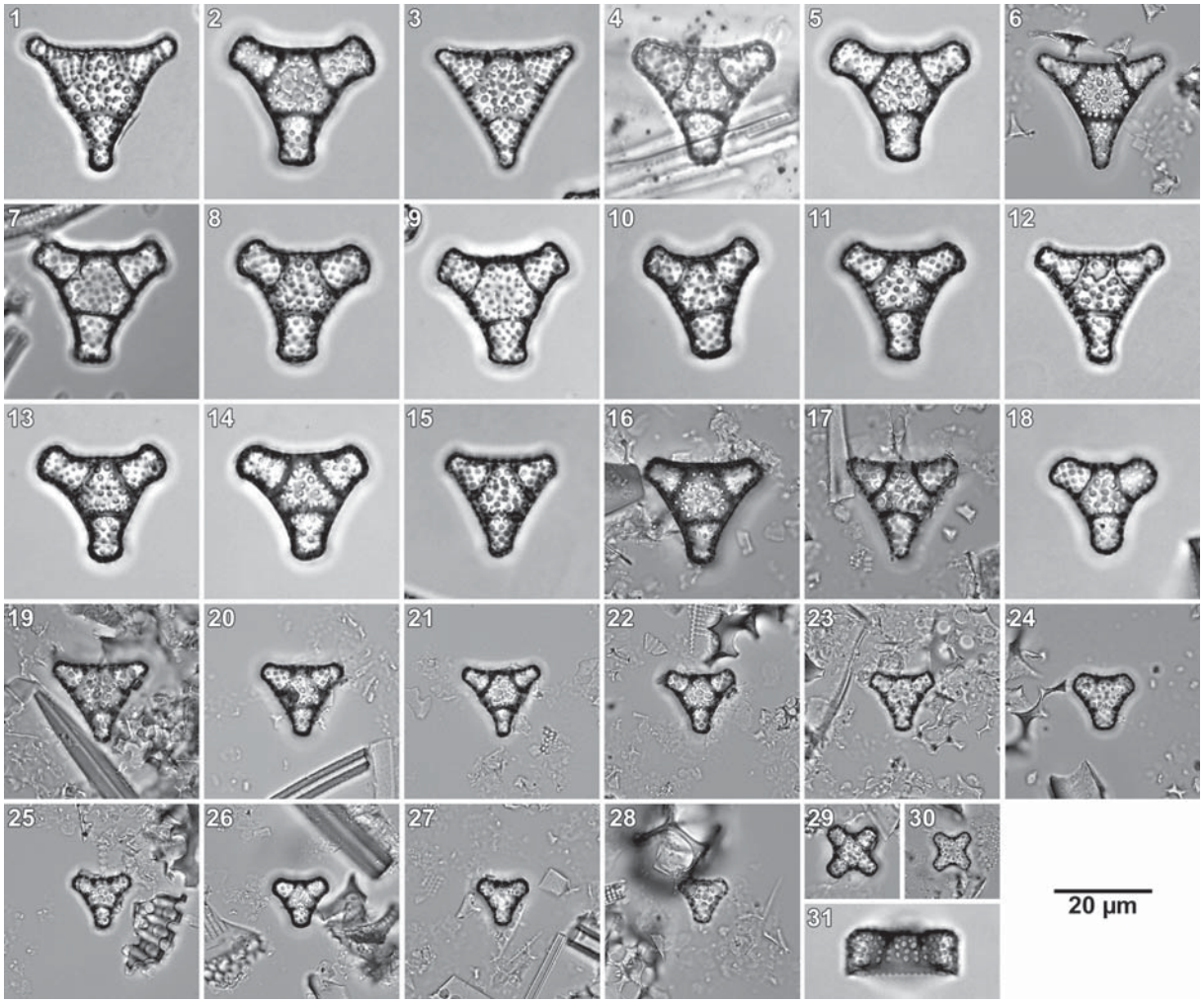
1
2
3
4
5
6
7
8
9
10
11
12
13
14
15
16
17
18
19
20
21
22
23
24
25
26
27
28
29
30
31
20 µm

PLATE 3

Scanning electron micrographs of *Fenneria kanayae* (Fenner) J. Witkowski, comb. nov.

1 – Oblique external view of a partly corroded valve; DSDP 1-6-3-3, 87−93 cm (Brigger Collection, CAS610596), Bermuda Rise

2 – Oblique external view of a smaller, well-preserved valve. Arrow indicates a set of cameo/intaglio linking structures at the lower left pole; DSDP 1-6-4-1, 57−63 cm (Brigger Collection, CAS 610598), Bermuda Rise

3 – Internal view of a tripolar valve. Note prominent pseudosepta extending from the poles toward the centre (white arrowhead) and the expanded distal edges of the internal costae, making a rounded triangular pattern (arrow), as well as the prominent serrations on the mantle margin (black arrowhead); Islas Orcadas Core 1678-48, 22−24 cm (SZCZ 18286), Falkland Plateau

4 – Slightly oblique internal view of a quadripolar valve. Note pseudosepta, less well-developed than in 3, and smaller expansion of the internal costae; DSDP 1-6-4-1, 57−63 cm (Brigger Collection, CAS 610598), Bermuda Rise

5 – Broken valve showing two levels of circumferential costae (white arrows) within projections located at mid-depth above polar pseudosepta (white arrowhead). Expanded distal edges of the internal costae produce a rounded triangular pattern in the centre (black arrow); DSDP 1-6-4-1, 57−63 cm (Brigger Collection, CAS 610598), Bermuda Rise

6 – Detail of 4, showing internal openings of the rimoportulae adjacent to internal costae, as indicated by arrows

7 – Internal view showing openings to rimoportulae located proximally adjacent to internal costae, and internal costae elevated to join with pseudopsepta creating a window, visible on the upper left pole; Islas Orcadas Core 1678-48, 22−24 cm (SZCZ 18286), Falkland Plateau

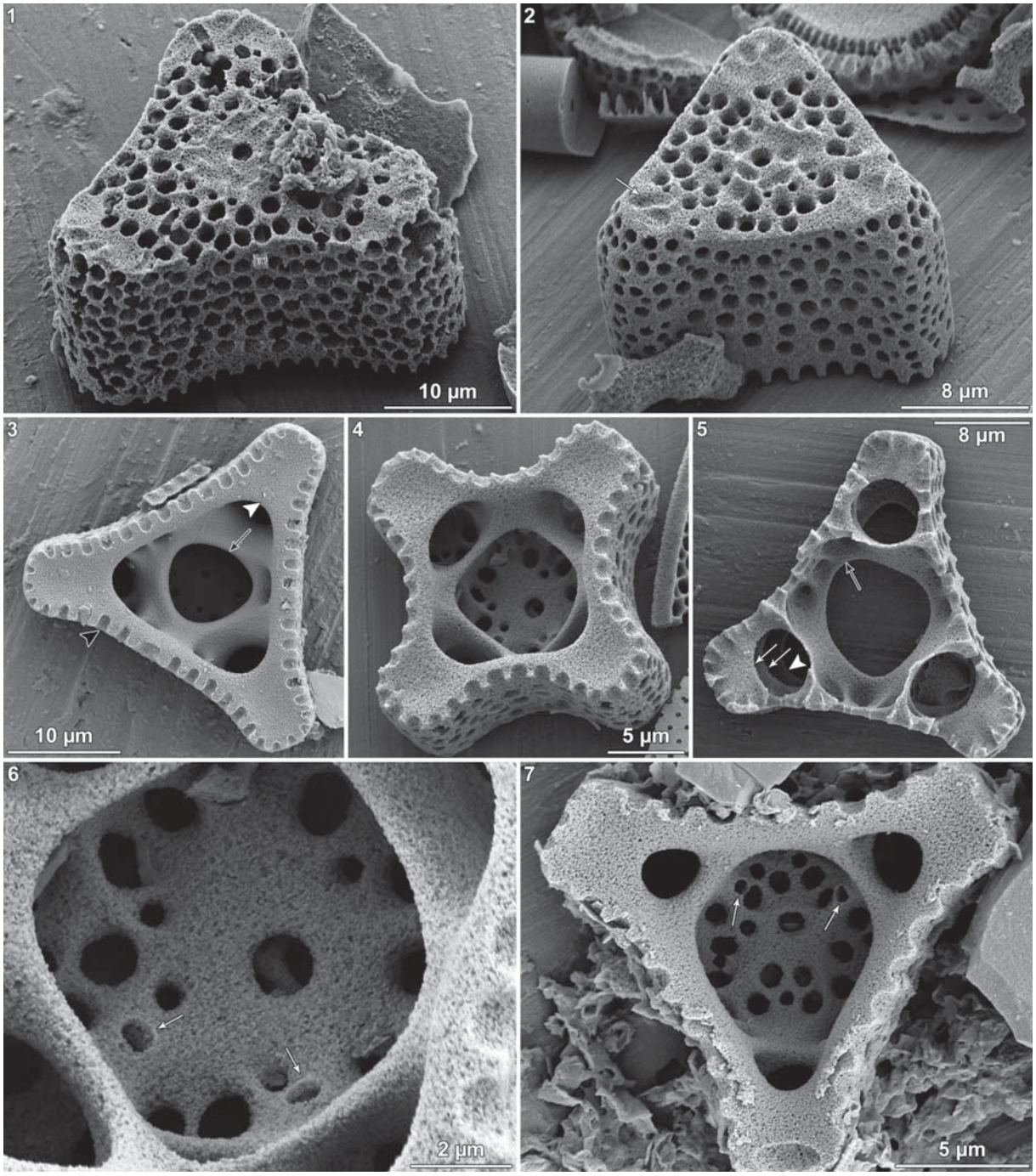
1
10 µm
2
8 µm
3
10 µm
4
5 µm
5
8 µm
6
2 µm
7
5 µm

PLATE 4

Light micrographs of *Fenneria kanayae* (Fenner) J. Witkowski, comb. nov.

1, 3-19 − External valve views. Arrows in 8, 10 and 14 point to internal radial costae; 1 − CAS 610598 (DSDP 1-6-4-1, 57−63 cm, Bermuda Rise); 3, 9-11, 13, 14, 18, 19 − SZCZ 23888 (DSDP 43-386-17R-1, 47−48 cm, Bermuda Rise); 4 − ODP 171B-1050A-9H-7, 34−35 cm (Blake Nose, MRC slide); 5 − CAS 610596 (DSDP 1-6-3-3, 87−93 cm, Bermuda Rise); 6, 8, 16 − SZCZ 23885 (DSDP 43-386-15R-3, 62−63 cm, Bermuda Rise); 7, 15, 17 − SZCZ 15222 (DSDP 39-356-9-1, 130−131 cm, São Paulo Plateau); 12 − SZCZ 21641 (ODP 171B-1051A-29X-3, 50−51 cm, Blake Nose)

2 − Internal valve view. Arrow indicates the proximal edge of polar pseudoseptum. SZCZ 23885 (DSDP 43-386-15R-3, 62−63 cm, Bermuda Rise)

20-21 − Girdle views; SZCZ 23885 (DSDP 43-386-15R-3, 62−63 cm, Bermuda Rise)

22 − Frustule in girdle view; SZCZ 23888 (DSDP 43-386-17R-1, 47−48 cm, Bermuda Rise)

23 − Sibling valves in girdle view; SZCZ 21652 (ODP 171B-1051A-40X-1, 50−51 cm, Blake Nose)

24 − Two specimens in internal valve view. White arrow points to proximal edge of circumferential internal costa; black arrows point to expanded distal edges of transverse internal costae; SZCZ 23885 (DSDP 43-386-15R-3, 62−63 cm, Bermuda Rise)

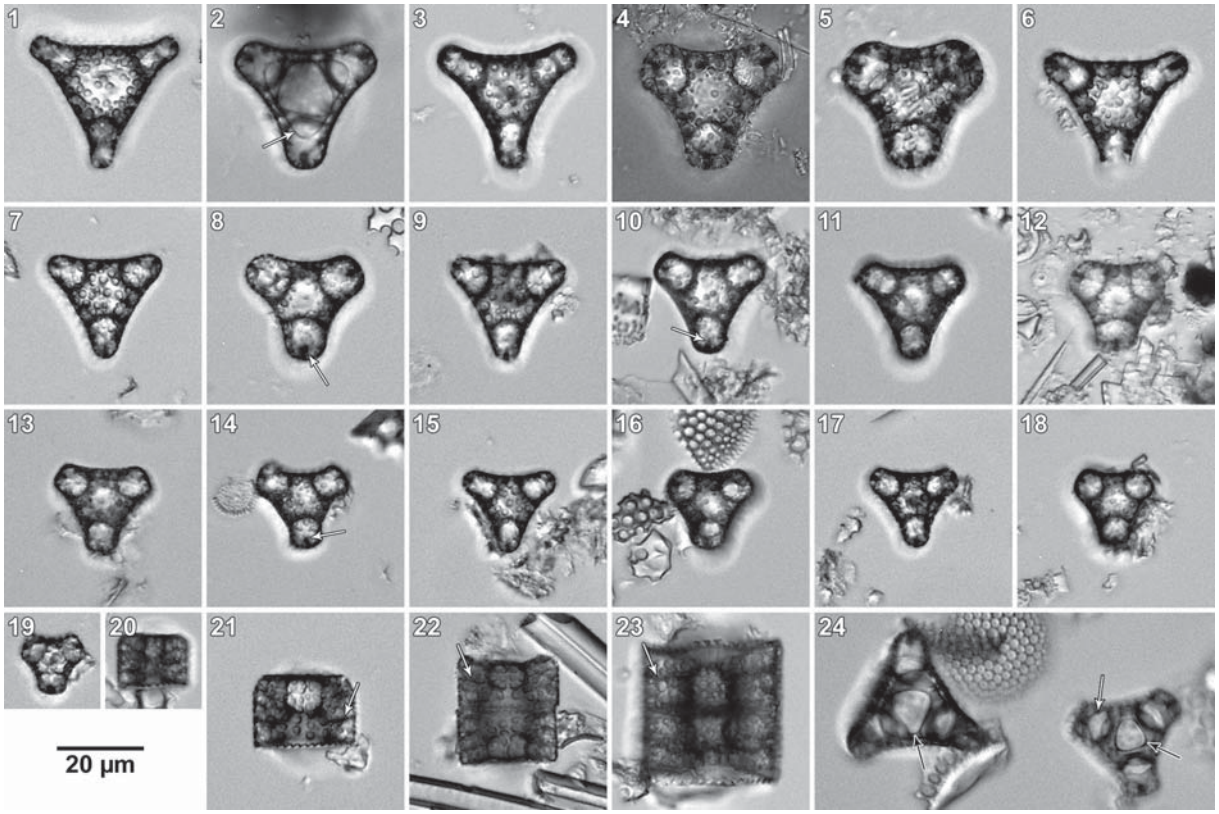
1
2
3
4
5
6
7
8
9
10
11
12
13
14
15
16
17
18
19
20
21
22
23
24
20 µm